Article:
Hager, J.R., Kugler, A.J., Kennedy, A.R. et al. (2026) Evaluating the extent of microbially-induced glass alteration by a subsurface Paenibacillus bacterium. npj Materials Degradation. ISSN: 2397-2106

https://doi.org/10.1038/s41529-026-00775-y

npj Materials Degradation

https://doi.org/10.1038/s41529-026-00775-y

Article in Press

Evaluating the extent of microbially-induced glass alteration by a subsurface *Paenibacillus* bacterium

Received: 15 October 2025

Accepted: 12 March 2026

Cite this article as: Hager, J.R., Kugler, A.J., Kennedy, A.R. *et al.* Evaluating the extent of microbially-induced glass alteration by a subsurface *Paenibacillus* bacterium. *npj Mater Degrad* (2026). https://doi.org/10.1038/s41529-026-00775-y

Jacqueline R. Hager, Alex J. Kugler, Ashley R. Kennedy, Andrew E. Plymale, José Marcial, Rachel M. Anguish, William Chrisler, David W. Hoyt, Tanya E. Winkler, Robert P. Young, Thomas W. Wietsma, Rossane C. Delapp, Lesa R. Brown, David S. Kosson, Clare L. Thorpe, James J. Neeway, Carolyn I. Pearce & Albert A. Kruger

Title: Evaluating the Extent of Microbially-Induced Glass Alteration by a Subsurface *Paenibacillus* Bacterium

Authors

Jacqueline R Hager[1] (jacqueline.hager@pnnl.gov), **Alex J Kugler[1]** (alex.kugler@pnnl.gov), **Ashley R Kennedy[1]** (ashley.kennedy@pnnl.gov), **Andrew E Plymale[1]** (plymale@pnnl.gov), **Jose Marcial[1]** (jose.marcial@pnnl.gov), **Rachel M Anguish[1]** (rachel.anguish@pnnl.gov), **William Chrisler[1]** (william.chrisler@pnnl.gov), **David W Hoyt[1]** (david.hoyt@pnnl.gov), **Tanya E Winkler[1]** (tanya.winkler@pnnl.gov), **Robert P Young[1]** (robert.young@pnnl.gov), **Thomas W Wietsma[1]** (wietsma@pnnl.gov), **Rossane C Delapp[2]** (rossane.c.delapp@vanderbilt.edu), **Lesa R Brown[2]** (lesa.brown@vanderbilt.edu), **David S Kosson[2]** (david.kosson@vanderbilt.edu), **Clare L Thorpe[3]** (clare.thorpe@sheffield.ac.uk), **James J Neeway[1]** (james.neeway@pnnl.gov), **Carolyn I Pearce[1]** (carolyn.pearce@pnnl.gov), **Albert A Kruger[4]** (albert.kruger@hanford.gov)

[1]Pacific Northwest National Laboratory, Richland, WA, USA

[2]Department of Civil and Environmental Engineering at Vanderbilt University, Nashville, TN, USA

[3]Department of Materials Science and Engineering at University of Sheffield, Sheffield, UK

[4]US Department of Energy, Hanford Field Office, Richland, WA, USA

Corresponding authors:

Jacqueline R Hager[1] (jacqueline.hager@pnnl.gov)

Carolyn I Pearce[1] (carolyn.pearce@pnnl.gov)

Abstract

Silicate glasses are an accepted option for immobilizing nuclear waste and waste glass can be disposed in near-surface environments. It is important to understand glass alteration mechanisms under site-relevant conditions to predict glass corrosion rates upon disposal. Microbial activity near the glass surface may influence glass alteration. However, waste glass chemical durability is currently evaluated without consideration of microbial alteration. Here, four glass compositions were tested in three solutions, with and without a subsurface *Paenibacillus* bacterium, to compare the extent of glass leaching. Results indicate that the *Paenibacillus* cells increased glass alteration, resulting in higher concentrations of boron, iron, sodium, and silicon released into solution. The combination of microbially mediated organic acid production, which decreased pH, and glass dissolution, which increased pH, resulted in a net neutral or slightly acidic solution that could promote further glass alteration. The amount of each element released depended on glass composition and solution chemistry. This study revealed the dynamic relationship between microbial metabolism, elemental release, and corresponding changes to solution pH, showing that microbial processes can indirectly accelerate glass alteration. This work supports a greater understanding of microbially-influenced glass alteration and informs development of standardized durability tests to assess microbial influence at disposal facilities.

Introduction

Glass is an amorphous (i.e., non-crystalline) solid formed by rapid melt quenching. Natural glasses exist in various forms, including obsidian, basaltic glass, Pele's hair, and fulgurite [1], while anthropogenic glasses have been created consistently for at least 4000 years [2]. Historically, glass has been used as window panes, jewelry, tableware, and blades, among other items [3, 4]. Another significant use of glass is through the vitrification of fission products from nuclear reactors. Research into vitrification as a waste form started in the 1950s and has evolved significantly in the last seven decades [5]. Based on this research, the US Department of Energy (DOE) selected vitrification as a preferred option for immobilizing radioactive liquids into a more stable, manageable form at the DOE Hanford Site, located in south-central Washington. At Hanford, legacy waste from plutonium production during the Cold War will be vitrified, and the low-activity waste (LAW) glass disposed onsite in the near-surface Integrated Disposal Facility (IDF) [6].

As the chemical durability of the LAW glass is directly related to the release of radionuclides into the near-field environment, there has been a tremendous amount of research on the long-term durability of glass, including the development of leach tests to evaluate glass formulations. These studies have examined the physicochemical changes that occur when glass interacts with water and with other environmental factors over time [7-9]. Studies have revealed several primary processes governing glass alteration, including hydration [10], ion exchange [11], hydrolysis [12], and condensation reactions [13], which lead to the formation of an alteration layer on the glass surface [14]. Research in this area has also led to the development of standardized test methods. There are standards for testing glass dissolution rate (ASTM C1662-18 and ASTM C1926-23) and glass waste form durability (ASTM C1663-18 and ASTM C1285-21), and environmental leaching (e.g., EPA-SW-846 method 1313 (2012), described further below). These tests are important to obtain a mechanistic understanding of glass alteration, and to evaluate the long-term behavior of different glass formulations in the environment, so that the performance of waste glass in a disposal facility can be assessed [15].

Some of the environmental factors that are less well researched are the interactions between microbes and glass, and how these interactions might affect both microbial communities and long-term glass durability. Microbial processes that occur at the interface between the glass and the near-surface environment may directly or indirectly affect glass alteration rates. Enzymes, proteins, organic acids, and metabolic processes can increase dissolution kinetics, and microbial biomineralization may affect the alteration products [16]. Previous work on microbe-mineral interactions has shown that having a surface to weather, such as minerals or glass, along with a source of additional nutrients, supports and influences the microbial population [16]. Minerals, including feldspars, micas, and clays, have been shown to release potassium, magnesium, iron, and phosphorus through weathering, which can enable microbial growth in low nutrient environments [17]. Similarly, Cockell *et al.* (2009) investigated microbial colonization of basaltic glass, which revealed diverse communities of Actinobacteria and Proteobacteria, among others, which were able to weather the substrate and exploit glass surfaces to access nutrients, including metal cations [18].

Microorganisms can also develop biofilms on surfaces, further influencing alteration processes through trapping moisture, the production of different metabolites, and the creation of microenvironments, which may be oxygen deficient or acidic [19, 20]. In oligotrophic (nutrient poor) environments, such as below the plant rooting zone in the Hanford vadose zone, limited energy is available for microbial metabolism, which will likely limit colonization near disposed vitrified waste [21]. Over thousands of years, groundwater intrusion could aid colonization despite limited carbon availability. This scenario is particularly plausible if waste is stored in steel containers, which may supply electron donors for autotrophic microorganisms [22, 23]. Likewise, if the vitrified waste contains some ferrous iron (Fe(II))- or manganese (Mn(II))-containing species, the wasteform itself could be a source of energy for microbial colonization by metal oxidizing prokaryotes [24, 25]. Facultative anaerobic organisms can generate energy via aerobic or anaerobic processes and can metabolize a wide variety of energy sources [26].

These microorganisms use available oxygen, then switch electron acceptors once oxygen becomes depleted in anoxic or microaerophilic microenvironments (e.g., biofilms). Altering subsurface environments and introducing new substrates (e.g., waste and oxygen) that support microbial life significantly alter subsurface microbiomes. These changes can unpredictably impact the entire ecosystem and are difficult to manage. Excavation exposes these microbiomes to oxygen, and once sealed, microaerophilic environments are likely to dominate at the near subsurface after extended periods of time [27].

To study the behavior of silicate glass waste forms over millennia time scales in near-surface environments, archeological glass artifacts can be used as analogs to evaluate glass alteration due to the natural environment [28]. Previous work from a recent excavation of Broborg, a Swedish vitrified hillfort, examined the interactions of the anthropogenic glass and surrounding rock with the native soil and subsurface microbial communities over the past ~1500 years [29-32]. Analyses of the glass revealed two compositions, (i) felsic (i.e., alkali and silica rich), and (ii) mafic, (i.e., iron rich), where the mafic glass samples showed signs of biological colonization [29, 32]. Subsequent microbial investigation of excavated glass samples found a niche community of microbes living in contact with the glass [30]. Since these glasses were altered under uncontrolled conditions in the environment, it is challenging to distinguish between chemical and biological alteration processes. To better understand these underlying processes, controlled laboratory experiments were needed to evaluate the effects of glass composition on microbial alteration by incorporating microbes with established physiochemical glass leaching test methods.

In this study, the role of a facultative anaerobic microorganism in the microbial induced alteration of glass is investigated by comparing rates and extent of glass leaching using a modified room temperature, pH-dependent leach test established by the United States Environmental Protection Agency (EPA) Leaching Environmental Assessment Framework (LEAF) (EPA-SW-846 method 1313, abbreviated “EPA 1313” herein) [33]. The four glass compositions used are 1) a simulated mafic (“Dark”) glass from the Swedish archaeological hillfort; 2) a simulated borosilicate LAW glass; and 3) two ‘join’ glasses that bridge the archeological glass composition with modern glasses by including boron and additional sodium. These glasses were tested in three solutions, 1) deionized water, 2) minimal microbial growth media, and 3) synthetic vadose zone porewater (VZPW) amended with specific microbial nutrients. The facultative anaerobic bacterial strain is a subsurface isolate of the *Paenibacillus* bacterial genus, which have been found in enriched rooting zones and have also been detected in biofilms growing on architectural and archeological glasses [30, 31, 34-36], and in the subsurface at the Hanford site [37]. Durability of the glasses, under initial oxic conditions, is examined in the presence and absence of bacteria at both the macroscale and microscale for 100 to 200 days. At selected time steps, solution and solid samples were removed from the original tube for analyses including pH, bacterial density, confocal laser microscopy (CLSM), cation analysis via inductively coupled plasma optical emission spectroscopy (ICP-OES), and analysis of bacterial metabolites using total carbon and nitrogen coupled with nuclear magnetic resonance (NMR). This research aims to address gaps in the understanding relating to microbial induced alteration of glass, and how it can potentially affect long-term glass stability.

Results

In this section, results from solutions analysis (pH, cell growth via optical density, total organic carbon, metabolic processes via nuclear magnetic resonance spectroscopy, and glass alteration via normalized elemental release) are presented as a function of the test media (DIW, depleted HOD, and VZPW-amended) and discussed in terms of the different glass compositions (Dark, Join(mid), Join, and LAWA44). Confocal laser scanning microscopy results showing the interaction between the glass and the microbes are also presented.

pH

Changes in pH can be caused by multiple factors, including the products of microbial metabolism (which can lower pH) and the dissolution of glass (which can raise pH). Initial and final pH values are provided in Table 1, and the time-dependent data for each solution is shown in Figure S1.

DIW. As shown in Table 1 and Figure S1, the pH of the solutions containing each of the four glasses increased over time. By 100 days, the glass-containing solutions with the lowest to highest pH were Dark (8.52), LAWA44 (9.65), Join(mid) (9.92), and Join (11.22) glass, respectively. The final pH is proportional to the leaching of sodium from the glass into solution (see "Normalized elemental release" in Results section). The DIW sample without glass did not change over time, remaining at pH ~6.1 for the 200-day duration (Table 1).

Depleted HOD. The pH of the abiotic solutions containing Dark, Join(mid), and LAWA44 glass remained stable at pH ~7.0 for the duration of the test (Table 1, Figure S1). However, the pH of the abiotic solutions containing Join glass increased over 200 days from pH 6.85 to 8.32. The biotic depleted HOD solutions containing Join(mid), LAWA44, and Dark glass decreased in pH over time, and after 100 days, the pH was similar for all three glasses: Join(mid) (5.58), Dark (5.61), and LAWA44 (5.65). In contrast, the pH in biotic solutions containing Join glass increased slightly over time, from 6.85 at 0 days to 7.17 at 100 days and 7.31 at 200 days. For all four glasses, the abiotic solutions containing glass had a higher final pH than the corresponding biotic solutions containing glass. The pH of abiotic solutions without glass remained at ~6.8, whereas biotic solutions without glass decreased to 4.93 after 2 days, then stabilized to approximately ~4.5 after 49 days and for the rest of the experiment. After 100 days (the longest time point for which all conditions can be compared), all the abiotic solutions, except those containing Join glass, remained at pH 6.9-7.1, while all biotic solutions, except those containing Join glass, decreased over time, with the solutions without glass decreasing the most.

VZPW-amended. After 100 days, the pH of the abiotic solutions containing Join(mid) and LAWA44 glass stabilized at ~8.1, while the pH of the abiotic solutions containing Join glass increased over time (7.85 initially to 8.70 at 100 days). In the biotic solutions containing Join(mid) and LAWA44 glass, the pH at 100 days decreased to 5.40 and 5.63, respectively (Table 1, Figure S1). The pH of the biotic solutions with Join glass decreased to 5.99 after 2 days, increased to 7.50 after 49 days, then decreased to 7.12 after 100 days. The pH of the abiotic solutions without glass remained at ~7.8, while the pH of the biotic solutions without glass decreased to ~5.0 by 49 days and stabilized at 5.01 at 100 days. Tumbling did not change the pH with respect to static conditions for solutions containing LAWA44 glass, both with and without microbes. The pH for both the tumbled and static solutions with LAWA44 glass at 100 days was ~8.1 without microbes and ~5.6 with microbes (Table 1). The pH changes with and without glass, and with and without microbes, were similar to those in depleted HOD, where biotic solutions with glass had the lowest final pH compared to the abiotic solutions with glass, and the lowest pH was in the biotic solutions without glass.

Table 1. Initial and final pH values for each glass by solution.

	Dark glass		Join(mid) glass		Join glass		LAWA44 glass		No-glass	
Solution	**Initial**	**Final**	**Initial**	**Final**	**Initial**	**Final**	**Initial**	**Final**	**Initial**	**Final**
DIW Abiotic, tumbled	6.2	8.6 ± 0.0**	6.2	9.9*	6.2	11.2 ± 0.0**	6.2	9.7 ± 0.1**	6.2	6.1 ± 0.2**
Depleted HOD Biotic, tumbled	6.9	5.6 ± 0.0**	7.0	5.6*	6.9	7.3 ± 0.0**	7.0	5.7 ± 0.0*	6.9	4.6 ± 0.0**
Depleted HOD Abiotic, tumbled	6.9	7.0**	7.0	7.1*	6.9	8.3**	7.0	7.2*	6.9	6.9**
VZPW-amended Biotic, tumbled	Not tested	Not tested	7.8	5.4 ± 0.1*	7.8	7.1 ± 0.1*	7.8	5.6 ± 0.0*	7.8	5.0 ± 0.0*
VZPW-amended Abiotic, tumbled	Not tested	Not tested	7.9	8.1 ± 0.0*	7.9	8.7 ± 0.0*	7.9	8.2*	7.9	7.9 ± 0.0*
VZPW-amended Biotic, static	Not tested	Not tested	Not tested	Not tested	Not tested	Not tested	7.8	5.7 ± 0.1*	7.8	5.2 ± 0.1*
VZPW-amended Abiotic, static	Not tested	Not tested	Not tested	Not tested	Not tested	Not tested	7.9	8.0 ± 0.0*	7.9	7.9 ± 0.0*

Final pH values are single replicates or averages of duplicate samples with ± standard deviations. Standard deviations of 0.0 were rounded for significant figures.
*Final pH at 100 days
**Final pH at 200 days

In summary, the biotic solutions without glass have the lowest final pH, and the abiotic solutions with glass have the highest final pH. Addition of glass to the biotic solutions increases the final pH, with the extent depending on the composition of the glass.

Dissolved Organic Carbon (DOC)

DOC analysis provides the concentration of carbon source and electron donor available in each sample, where the consumption of DOC over time indicates microbial activity, which can be correlated with the optical density and NMR results. The initial DOC concentration in the depleted HOD and VZPW-amended solutions was ~3.3 g/L, with an additional ~0.9 g/L DOC added via periodic media supplementations (see "Solution preparation" section in Methods) by 100 days. The final DOC concentrations are provided in Table 2.

Depleted HOD. The DOC concentrations at 100 days ranged from 4.33 g/L in abiotic solutions containing LAWA44 glass, down to 3.67 g/L in biotic solutions containing LAWA44 glass. For the three glass-containing samples, the abiotic solutions had highest DOC concentrations, consistent with no conversion of glucose to CO_2. The biotic solutions had lowest DOC concentrations, consistent with conversion of glucose to biomass that would be retained by the 0.2 µm filters and not present in the filtrate used for analysis. However, in the absence of glass, the biotic solutions had higher DOC concentrations than the abiotic solutions, which could be due to increased presence of metabolites (e.g. lysed cells or extracellular polymeric substances) passing through the 0.2 µm filter. The abiotic versus biotic solutions containing LAWA44 glass had the greatest difference in DOC concentration, and abiotic versus biotic solutions containing Join(mid) glass had the smallest difference in DOC concentration. For the biotic solutions containing glass, the DOC concentrations decreased from Join(mid), to Join, then LAWA44.

VZPW-amended. The DOC concentrations at 100 days ranged from 3.40 g/L in abiotic solution containing Join glass, to 2.58 g/L in biotic solution containing LAWA44 glass. For all samples, with and without glass, the abiotic solutions had greater DOC than the corresponding biotic samples, consistent with biotic conversion of glucose to biomass. The relative difference in DOC concentration between the abiotic and biotic samples with glass was largest in solutions containing Join glass and smallest in solutions containing LAWA44 glass. As in the depleted HOD solutions, the DOC concentrations in biotic VZPW-amended solutions containing glass decreased from Join(mid), to Join, then LAWA44.

Table 2. Dissolved organic carbon (DOC) (g/L) in < 0.2 μm filtrates for each glass by solution at 100 days. Maximum DOC added was 4.2 g/L. DOC for Dark glass and DIW were not measured. Samples were measured as single replicates, instrument uncertainty is approximately 5% of the reported value.

	Dissolved Organic Carbon (g/L)			
Solution	**Join(mid) glass**	**Join glass**	**LAWA44 glass**	**No glass**
Depleted HOD Biotic, tumbled	3.89	3.82	3.67	4.21
Depleted HOD Abiotic, tumbled	3.99	4.20	4.33	3.96
VZPW-amended Biotic, tumbled	2.78	2.66	2.58	2.63
VZPW-amended Abiotic, tumbled	3.37	3.40	3.12	2.84
VZPW-amended Biotic, static	Not tested	Not tested	2.93	2.98
VZPW-amended Abiotic, static	Not tested	Not tested	3.04	2.76

In summary, while the trends in DOC are more challenging to interpret due to the use of HEPES (organic buffer) for pH control in depleted HOD, and the potential for cell lysis in biotic solutions, the DOC concentrations were generally lower in biotic solutions compared to the corresponding abiotic solutions. This is consistent with microbial activity consuming glucose. Addition of glass enhanced microbial activity, resulting in more glucose consumption and a further decrease in DOC concentration when compared to the corresponding abiotic samples.

Optical Density

Optical density measurements at 600 nm (OD_{600}) provide an estimate of the concentration of cells, showing cell growth (reported as a dimensionless arbitrary unit) over time and how it is impacted by the solution conditions and the presence or absence of glass. Initial and final OD_{600} are provided in Table 3, and the time-dependent data for each solution are shown in Figure S2. All abiotic solutions with and without glass only had OD_{600} values close to background, indicating no biological growth. Abiotic DIW samples were not sampled for OD_{600} measurements, but none of the samples showed any visual signs of biological growth or contamination.

Depleted HOD. The OD_{600} for biotic solutions containing glass increased over time and were as follows after 100 days: (i) Join(mid) or LAWA44, 0.15; (ii) Join glass, 0.20; and (iii) Dark glass, 0.23. The OD_{600} for the biotic depleted HOD solution containing Join glass was measured at multiple time points and decreased from 0.38 at 2 days to 0.12 at 49 days, but increased to 0.37 by 200 days, with a similar trend observed in the biotic solutions without glass. At 100 days, the OD_{600} of the biotic solution without glass was 0.13, and increased to 0.18 after 200 days, which was lower than the solutions with glass.

VZPW-amended. After 100 days, the OD_{600} for biotic solutions containing glass were as follows: (i) Join(mid) glass, 0.24; LAWA44 glass. 0.18; and Join glass, 0.13. The OD_{600} for the biotic VZPW-amended solutions containing Join glass showed a biomass spike at 2 days, followed by a decrease at 49 days, as with the depleted HOD solutions. After 100 days, the tumbled solutions had greater biomass than the static solutions, both with LAWA44 and without glass. At 100 days, the OD_{600} of the biotic solution without glass was 0.20.

Table 3. Initial and final optical densities (OD_{600}) for each glass by solution. OD_{600} for DIW was not measured since no microbes were added as part of the DIW test.

	Dark glass		Join(mid) glass		Join glass		LAWA44 glass		No glass	
Solution	**Initial**	**Final**	**Initial**	**Final**	**Initial**	**Final**	**Initial**	**Final**	**Initial**	**Final**
Depleted HOD Biotic, tumbled	0.002	0.45 ± 0.03**	0.005	0.15*	0.002	0.37 ± 0.01**	0.005	0.15 ± 0.00*	0.002	0.18 ± 0.01**
Depleted HOD Abiotic, tumbled	0.000	0.000**	0.000	0.000*	0.000	0.000**	0.000	0.000*	0.000	0.000**
VZPW(amended) Biotic, tumbled	Not tested	Not tested	0.004	0.24 ± 0.01*	0.004	0.13 ± 0.04*	0.004	0.18 ± 0.01*	0.004	0.20 ± 0.01*
VZPW(amended) Abiotic, tumbled	Not tested	Not tested	0.001	0.000*	0.001	0.000*	0.001	0.000*	0.001	0.000*
VZPW(amended) Biotic, static	Not tested	Not tested	Not tested	Not tested	Not tested	Not tested	0.004	0.11 ± 0.01*	0.004	0.14 ± 0.02*
VZPW(amended) Abiotic, static	Not tested	Not tested	Not tested	Not tested	Not tested	Not tested	0.001	0.000*	0.001	0.000*

Final optical density values are single replicates or averages of duplicate samples with ± standard deviations.
*Final optical density at 100 days
**Final optical density at 200 days

In summary, the OD_{600} was higher in the presence of glass in some cases, where tumbled tests generally resulted in higher OD_{600} than static tests, and VZPW-amended solutions had higher OD_{600} than depleted HOD solutions except in the presence of Join glass.

Confocal Laser Scanning Microscopy (CLSM)

Imaging the post-experiment glass samples with CLSM provided a qualitative evaluation of the *Paenibacillus* cells and their association with the glass particles, either as planktonic cells in the surrounding solution or attached to the glass. Images were captured at the final sampling point for each of the biotic and abiotic glasses. Glass samples were imaged twice: (i) as-is from the original tube, and (ii) after "washing" the glass with fresh depleted HOD or VZPW-amended solution. This "wash" step would dislodge any biofilm only loosely associated with the powders. See Figure 1 (depleted HOD) and Figure 2 (VZPW-amended) for the original, unwashed glass samples. Images of the washed glasses are given in Figure S3 and Figure S4. Figure S5 provides a zoom into one of the stitched CLSM images for added viewing clarity.

Depleted HOD. The original biotic Dark glass showed dense microbial growth, but most of the *Paenibacillus* cells appeared to be between the glass particles (Figure 1A). After washing, only a few *Paenibacillus* cells remained in the surrounding solution, with sporadic cells attached to individual glass particles (Figure S3A). The biotic Join(mid) glass appeared to have fewer cells than the Dark glass, and they were mostly between the glass particles (Figure 1C). The biotic LAWA44 glass (Figure 1G) had fewer visible cells than the Dark or Join(mid) glasses, and the cells were mostly in clusters, in contrast to the dispersed cells observed with the Dark and Join(mid) glasses. Some individual cells were associated with the LAWA44 glass particles, whereas the cell clusters were only in suspension. Since very few cells were observed in the washed Dark, Join(mid), and LAWA44 glass samples (Figure S3), most of the biofilm was not directly associated with these glass samples and remained in the wash solution.

The biomass on the biotic Join glass (Figure 1E) was denser than the other glass samples, which agreed with the optical density measurements, and there were many octahedrally-shaped particles, approximately 10-20 μm in length, throughout the sample. The particles appeared green due to autofluorescence and not from the SYBR gold stain, i.e., they did not contain DNA. This is because the SYBR gold stain is highly selective for DNA molecules and the fluorescent signal from the particles was much greater than the corresponding signal from the *Paenibacillus* cells, which suggests autofluorescence.

Some spores were also observed, indicating the microbes were under stress. The washing step removed most cells and particles (Figure S3C). A sample of the wash solution was examined under the microscope (no images captured), showing that some of these octahedrally-shaped particles were still present in the solution, i.e., they did not dissolve in the fresh depleted HOD solution.

The corresponding abiotic glass samples (Figure 1, panels B, D, F, and H) showed no microbial signatures, consistent with the optical density measurements.

VZPW-amended. The biotic Join(mid) glass (Figure 2C) had dense cell clusters and a few individual *Paenibacillus* cells. After washing, most of the cell clusters were removed, but the single *Paenibacillus* cells were still present and most likely attached to the glass particles (Figure S4A). The biotic Join glass (Figure 2A) had less dense biomass, consisting mostly of cells between the glass particles. As with the biotic Join glass in the depleted HOD solution, numerous octahedrally-shaped particles were present. The washing step removed most of the microbes and particles, but some microbes remained adhered to the glass (Figure S4C).

The tumbled biotic LAWA44 glass (Figure 2E) contained densely packed cells, with cell clusters and individual cells present, but none of them appeared to be associated with the glass particles. This was confirmed when all of the cells were removed in the washing step (Figure S4E). The static biotic LAWA44 sample (Figure 2G) had much less biomass than the tumbled sample, but the biomass consisted of similar cell clusters. However, in contrast to the tumbled sample, it was clear that some of the biomass was associated with the glass particles. The washing step removed most of the cell clusters, but the single cells that adhered to the glass remained (Figure S4G).

The corresponding abiotic glass samples (Figure 2, panels B, D, F, and H) showed no microbial signatures, consistent with the optical density measurements.

Nuclear Magnetic Resonance (NMR) Spectroscopy

NMR spectroscopic analysis provides identification and quantification of abiotic glass leachate and biotic compounds, reaction intermediates, and amino acid content. Initial and final metabolite concentrations are in Table 4 to Table 7 and the time-dependent data for each solution are in Figure 3, Figure 4, Figure S6, and Figure S7. The NMR analysis of the solution supernatants revealed the presence of 33 separate organic compounds in depleted HOD (Table S1) and 41 separate organic compounds in VZPW-amended (Table S1). Of those compounds, seven were identified as prominent metabolic markers, including acetate, acetoin, butyrate, ethanol, formate, glucose, and lactate (Table 4, Table 6, Figure 3, and Figure 4). Glucose was added during the experiment as the primary carbon source and was likely utilized for the fermentative processes listed above [53]. Acetate and formate are both indicators of mixed-acid fermentation pathways [54]. Acetoin, butyrate, and ethanol are indicators of anaerobic fermentation [55]. Lactic acid products, including lactate, ethanol, and carbon dioxide, are associated with heterolactic fermentation [53]. A complete list of acidic compounds is indexed with final pH values in Table S2 and Table S3. The amino acid contents (Table 5 and Table 7) were analyzed to determine possible metabolic outliers among the samples [56]. Note, as stated in the "Modified EPA 1313 Glass Corrosion Tests" section in Methods, 70% ethanol was used in the BSC to maintain aseptic conditions, which likely carried over into the subsamples for NMR, given that all of the solutions contained a minimum of 250 μM ethanol. It was not possible to correct for this due to the variability of the ethanol content in the abiotic solutions with and without glass, so the qualitative trends are discussed.

Depleted HOD. Glucose and lactate showed an inverse relationship in the biotic solutions. As the amount of glucose in solution decreases, the amount of lactate increases, likely due to glycolysis under anaerobic conditions, where lactate is a byproduct [53]. After 100 days, the lactate concentration in the biotic Join(mid) glass solution and in the biotic LAWA44 glass solution had increased to 109 μM and 272 μM, respectively. Over 200 days, lactate production was the highest in the biotic Join glass solution, increasing

from 54 to 588 μM, followed by the biotic solution without glass, increasing from 135 to 233 μM. The abiotic solutions contained only trace concentrations of lactate, while the glucose concentration increased according to the amount added over time. The glucose concentrations in the abiotic solutions were 6.3 ± 1.2 mM at 2 days, 14.6 ± 1.6 mM at 49 days, and 27 ± 0.7 mM at 200 days.

All biotic solutions contained acetate, with a general trend of increasing acetate concentration from the initial to final time points, suggesting that the *Paenibacillus* did not oxidize acetate under these conditions. After 100 days, the LAWA44 glass solution contained 3.7 mM acetate, and the Join(mid) glass solution contained 1.1 mM acetate. The acetate concentration in the Join glass solution increased from 1.4 mM after 2 days to 15 mM after 200 days. The acetate concentration in the depleted HOD solution without glass only increased from 0.6 mM after 2 days to 2.5 mM after 200 days. The Dark glass solution contained a similar acetate concentration (2.2 mM) after 200 days. All abiotic solutions contained only trace amounts of acetate (0.02 mM at the initial 2-day sampling and 0.02-0.06 mM at the final 100 or 200-day samplings).

Formate concentrations were highest in the biotic Join glass solution, with 1032 μM at 49 days and 973 μM at 200 days and were significantly less in the abiotic Join glass solution (54 μM at 200 days). Formate was also present in the Dark glass solutions after 200 days, with 146 μM in the biotic and 96 μM in the abiotic solutions. Formate concentrations were lower in the LAWA44 glass solutions after 100 days, with 66 μM in the biotic and 11 μM in the abiotic solutions. The Join(mid) glass solutions and the solutions without glass (biotic and abiotic) had formate concentrations of < 40 μM at the final time point.

The biotic solutions also contained acetoin, a known chelating agent and alkoxide stabilizer [57]. Acetoin was not generally present until 49 days or later, and all biotic solutions showed increasing acetoin concentration, except the solution without glass, for which the acetoin concentration (30 μM) remained constant after 49 days. The acetoin concentration in the Join glass solution increased from 4 μM after 2 days to 231 μM after 200 days. After 100 days, the acetoin concentrations in the Dark, Join(mid), and LAWA44 glass solutions were 13 μM, 25 μM, and 98 μM, respectively. All abiotic solutions contained ≤ 2 μM acetoin.

Trace amounts of butyrate were measurable in most solutions after 100 days, with similar concentrations in both biotic and abiotic solutions, ranging from 1.3 μM to 5 μM.

The highest ethanol concentrations were in the biotic Join glass solutions, and they continually increased throughout the experiment. The ethanol concentrations in the other biotic glass solutions followed similar increasing trends. By the final time point, the abiotic solutions with and without glass contained similar concentrations of ethanol (0.62-0.76 mM).

Amino acid content varied with glass type. Due to the addition of casamino acids throughout the experiment, including at the initial time point, 49 days, 100 days, and 200 days, amino acid content was normalized to percent composition. A selection of amino acids is provided in Table 5, while a full list of the amino acids in the casamino acids can be found in Table S4. Most samples showed an absence of arginine, lysine, and tyrosine, with a few exceptions. Arginine was only present in the biotic and abiotic LAWA44 glass solutions. Lysine was present in all of the 200-day abiotic solutions but was absent from the 2-day abiotic and biotic solutions. Tyrosine was only present in the biotic and abiotic Join(mid) and LAWA44 glass solutions. All final solutions consisted of a minimum of 21.7% glutamate and 10.1% proline, with the exception of the biotic Join glass sample, which had the lowest amino acid content, as seen in Table 5, with all but three amino acids being absent.

Table 4. A selection of metabolites detected in the depleted HOD solutions at the final time point.

	Dark glass**		Join(mid) glass*		Join glass**		LAWA44 glass*		No glass**	
	Biotic	**Abiotic**	**Biotic**	**Abiotic**	**Biotic**	**Abiotic**	**Biotic**	**Abiotic**	**Biotic**	**Abiotic**
Acetate (μM)	2215	50	1097	20.9	15265	59	3721	26.5	2540	42
Acetoin (μM)	13.4	2	25	0.9	231	0	97.9	0	35.8	1.7
Butyrate (μM)	5	0	4.5	1.3	0	0	4.1	3.5	0	0
Ethanol (mM)	0.86	0.70	0.84	0.76	2.15	0.67	0.99	0.67	0.69	0.62
Formate (μM)	146	96	21.5	10.1	973	54	65.7	10.8	24	36.9
Glucose (mM)	24.9	29.3	11.3	19.2	0	26.6	6.8	19.5	25.6	27.5
Lactate (μM)	41.8	0	109	6.6	588.3	0	271.9	6	232.8	0

*Final concentrations at 100 days
**Final concentrations at 200 days

Table 5. Amino acid content (% of total) in depleted HOD solutions at 2 and 100 or 200 days.

	Day 2		Day 100				Day 200					
Amino Acid	**Biotic, no glass**	**Abiotic, no glass**	**Biotic, Join(mid)**	**Abiotic, Join(mid)**	**Biotic, LAWA44**	**Abiotic, LAWA44**	**Biotic, no glass**	**Abiotic, no glass**	**Biotic, Dark**	**Abiotic, Dark**	**Biotic, Join**	**Abiotic, Join**
Alanine	18.90	9.40	8.51	8.04	13.06	8.09	10.50	8.07	11.78	8.39	41.25	8.19
Arginine	-	-	7.36	-	4.26	0.98	-	-	-	-	-	-
Aspartate	20.79	14.52	5.38	12.74	10.70	9.29	14.35	14.48	11.22	10.75	-	-
Glutamate	57.09	27.48	29.59	22.75	36.95	24.17	31.23	25.99	21.76	25.54	-	30.12
Isoleucine	-	3.93	3.45	4.51	2.79	4.88	4.08	4.33	4.65	5.82	-	5.18
Leucine	-	10.05	6.08	11.07	3.08	11.02	8.82	12.12	11.88	13.09	-	13.17
Lysine	-	-	-	8.04	-	10.00	-	6.17	-	-	-	7.02
Methionine	-	1.19	1.63	2.58	2.24	2.61	-	2.73	2.80	2.90	-	2.41
Phenylalanine	-	3.21	3.04	3.82	1.90	3.63	3.40	3.47	3.96	3.44	-	3.59
Proline	-	18.02	23.97	14.14	20.66	12.25	14.74	10.11	19.36	16.96	56.35	18.64
Threonine	-	5.65	4.32	3.09	-	3.88	5.87	5.25	5.61	5.22	-	4.75
Tyrosine	-	-	1.91	2.34	1.13	2.25	-	-	-	-	-	-
Valine	3.21	6.54	4.75	6.87	3.23	6.96	7.02	7.28	7.00	7.90	2.40	6.92
Total amino acid (μM)	52.9	168.1	460.6	507.7	405.7	510.2	806.4	912.9	697.2	817.7	245.6	820.7

VZPW-amended. As with the depleted HOD solutions, glucose and lactate showed an inverse relationship in the biotic VZPW-amended solutions. In the biotic LAWA44 glass solutions, lactate production (1.5 mM) was highest over 49 days, but decreased to 0.8 mM after 100 days. This decrease in lactate concentration from 49 to 100 days indicates that the *Paenibacillus* may have used the lactate as an electron donor, which it has been shown to do under anaerobic conditions [37]. In the biotic Join glass solution, glucose consumption was highest (concentration decreased to 1.2-1.9 mM) and lactate production reached 0.9-1.3 mM after 100 days. The concentration of lactate in the biotic solution without glass was 0.7 mM after 100 days. The abiotic solutions contained only trace concentrations of lactate (< 7 μM) and the glucose concentrations increased according to the amount added over time: 7.5 ± 0.3 mM at 2 days, 11.6 ± 0.4 mM at 49 days, and 18.7 ± 1.6 mM at 100 days.

After 2 days, all biotic solutions contained significant concentrations of acetate, a known chelating agent [57], and concentrations generally increased over time. The LAWA44 glass solution had the largest increase in acetate concentration from 0.5 mM after 2 days to 5.3 mM after 100 days. The acetate concentration in the Join glass solution decreased from 1.9 mM after 2 days to 1.5 mM after 49 days, then increased to 3.5 mM after 100 days. The acetate concentration in the Join(mid) glass solution was 1.7 mM after 100 days. The acetate concentration in the biotic solution without glass increased from 2.4 mM after 2 days to 4.3 mM after 100 days. All abiotic solutions contained < 28 μM of acetate.

Formate concentrations in the biotic solutions generally increased over time, with the LAWA44 glass solution having the highest concentration of 1795 μM after 100 days. All abiotic samples contained < 31 μM of formate.

All biotic solutions contained acetoin after 2 days and showed increasing amounts up to 100 days. At 100 days, the Join glass solution contained the most acetoin at 74 μM, followed by the solution without glass (39 μM), LAWA44 glass solution (33 μM), and Join(mid) glass solution (12 μM). All abiotic samples contained trace amounts of acetoin.

Small concentrations of butyrate (1 μM to 4.3 μM) were present in all solutions, both biotic and abiotic. The biotic Join glass solution contained the highest concentration of butyrate, increasing from 6 μM after 2 days to 30 μM after 100 days.

The ethanol concentrations in the biotic Join glass solution continually increased over time, but the biotic solution without glass reached the highest ethanol concentration after 100 days. The abiotic solutions all had ethanol concentrations of 0.73-0.74 mM, likely from peripheral 70% ethanol use when subsampling in the BSC for the NMR samples.

Amino acid content varied with glass type and presence of microbes. Due to the addition of casamino acids throughout the experiment, i.e., the initial time point, 49, and 100 days, sample contents were normalized to percent composition. A full list of casamino acid content can be found in Table S4. All abiotic samples displayed an absence of arginine, except for the LAWA44 glass solution, which contained 1% arginine. Final abiotic samples ranged from 461.5 to 521.6 μM total amino acid content. All biotic solutions displayed an absence of lysine. Final biotic samples ranged from 283.4 to 608.1 μM in total amino acid content. All solutions, regardless of the presence of glass or microbes, consisted of a minimum of 23% glutamate and 9.5% proline.

Table 6. A selection of metabolites present in the VZPW-amended solutions at the final time point.

	Join(mid) glass		**Join glass**		**LAWA44 glass**		**No glass**	
	Biotic	**Abiotic**	**Biotic**	**Abiotic**	**Biotic**	**Abiotic**	**Biotic**	**Abiotic**
Acetate (μM)	1703.7	24.5	11.6	24.8	2.7	27.5	4273	24.3
Acetoin (μM)	11.6	0.5	73.5	0.4	32.6	0.6	38.9	0.9
Butyrate (μM)	2.7	0	29.5	1.8	0	4.3	2.7	3.5
Ethanol (mM)	0.72	0.73	1.26	0.74	1.39	0.74	2.44	0.74
Formate (μM)	94.9	16.4	237.5	29.9	1795.2	30.2	1183.1	19
Glucose (mM)	10.30	18.28	1.91	18.39	10.14	18.57	13.87	19.05
Lactate (μM)	310.4	6.5	2.5	1092.2	1250.3	6.1	681.8	2.7

Table 7. Amino acid content in VZPW-amended solutions at 2 and 100 days.

	Day 2		Day 100							
Amino Acid	Biotic, no glass	Abiotic, no glass	Biotic, no glass	Abiotic, no glass	Biotic, Join	Abiotic, Join	Biotic, Join (mid)	Abiotic, Join(mid)	Biotic, LAWA44	Abiotic, LAWA44
Alanine	14.17	7.98	14.54	7.15	1.98	7.57	12.05	8.84	19.14	8.45
Arginine	9.40	-	8.34	-	1.76	-	9.99	-	4.00	1.02
Aspartate	13.26	8.22	10.74	8.19	-	5.52	5.50	7.71	4.11	14.90
Glutamate	34.20	26.70	27.48	26.71	45.17	27.97	23.06	25.48	34.65	25.23
Isoleucine	1.78	4.40	2.99	4.87	0.88	5.32	3.38	5.01	2.61	5.10
Leucine	2.69	11.27	7.12	12.27	3.39	12.85	6.55	12.05	6.22	11.50
Lysine	-	7.04	-	7.75	-	7.63	-	6.33	-	4.17
Methionine	-	2.46	2.10	1.76	-	2.23	1.44	2.84	2.15	2.86
Phenylalanine	0.39	3.52	2.29	3.57	3.95	3.73	3.17	4.20	1.92	3.79
Proline	15.49	14.96	12.22	14.32	40.40	15.00	23.58	14.41	17.31	9.49
Threonine	-	3.40	4.85	4.37	-	4.58	3.21	3.40	-	4.71
Tyrosine	0.65	2.70	1.84	2.45	1.55	1.75	1.81	2.49	1.83	2.35
Valine	7.97	7.34	5.49	6.60	0.92	5.86	6.26	7.24	6.06	6.43
Total amino acids (μM)	308.5	170.4	608.1	521.6	283.4	498.1	485.6	461.5	432.6	488.7

Normalized elemental release

The normalized elemental release is a measure of the mass of glass that has been released into solution. The elemental release was normalized according to the composition of each glass and surface-area-to-volume ratio of the glass powders (see Equation 1). The solutions without glass were used to determine the background elemental concentrations and subtracted from the glass containing solution data. Thus, only results for glass containing solutions are presented. The normalized release of selected elements (boron, iron, sodium, and silicon) for each solution containing glass at 100 days is shown in Table 8 to Table 11. Time dependent data grouped by element, with panels for each glass, are shown in Figure 5 to Figure 8. For the depleted HOD solutions, subsamples were collected at 2, 4, 7, 14, 28, 49, 100, and 200 days. For the VZPW-amended solutions, subsamples were collected at 2, 7, 14, 28, 49, and 100 days. The complete set of normalized elemental release data is provided in Table S5 to Table S7. The concentrations of the selected elements (boron, iron, sodium, and silicon) from the ICP-OES analysis are provided in Table S8 to Table S11.

DIW. At 100 days in DIW, the order of overall normalized elemental release from greatest to least was Join, Join(mid), LAWA44, and Dark glass, respectively (Table 8). For boron (Figure 5), the two join glasses released the same amount (0.22 g/m^2), which was five times the normalized released from the LAWA44 glass (0.04 g/m^2). The Dark glass composition did not include boron. For iron (Figure 6), the normalized release was similar across all the glass compositions, ranging from 0.02 g/m^2 for Dark glass to 0.07 g/m^2 for LAWA44 glass. For sodium (Figure 7), the two join glasses had the greatest release, 0.16-0.20 g/m^2, followed by LAWA44 glass at 0.12 g/m^2, and Dark glass at 0.06 g/m^2. For silicon (Figure 8), all of the glasses reached a similar release, ranging from 0.03 g/m^2 for Dark glass to 0.08 g/m^2 for Join glass, indicating that silicon is solubility controlled. Generally, the boron and sodium releases were an order of magnitude greater than the iron and silicon for both join glasses. However, the Dark glass maintained very low releases for all elements, from 0.02 g/m^2 for iron to 0.06 g/m^2 for sodium.

Table 8. Normalized release of selected elements in glass containing DIW solutions at 100 days. Note: biotic samples were not prepared for this solution, and the Dark glass composition did not contain boron.

	Normalized release (g/m^2) at 100 days							
	Dark glass		Join(mid) glass		Join glass		LAWA44 glass	
Element	**Biotic**	**Abiotic**	**Biotic**	**Abiotic**	**Biotic**	**Abiotic**	**Biotic**	**Abiotic**
Boron (B)	Not present	Not present	Not tested	0.22*	Not tested	0.22 ± 0.005	Not tested	0.04 ± 0.001
Iron (Fe)	Not tested	0.02 ± 0.000	Not tested	0.05*	Not tested	0.03 ± 0.001	Not tested	0.07 ± 0.001
Sodium (Na)	Not tested	0.06 ± 0.004	Not tested	0.16*	Not tested	0.20 ± 0.004	Not tested	0.12 ± 0.005
Silicon (Si)	Not tested	0.03 ± 0.003	Not tested	0.07*	Not tested	0.08 ± 0.002	Not tested	0.06 ± 0.003

Values are single replicates (*) or averages of duplicate samples with ± standard deviations.

Depleted HOD. After 100 days, the Join glass, in both biotic and abiotic treatments, had the greatest overall normalized elemental release in depleted HOD, followed by LAWA44 glass, Join(mid) glass, and Dark glass (Table 9). Biotic glasses had a greater normalized release of all elements than the corresponding abiotic glasses; however, the relative difference was glass composition- and time-dependent. Under all conditions, the Join glass released substantially more boron after 100 days than the Join(mid) and LAWA44 glasses (Figure 5). The biotic Dark, Join(mid), and Join glass treatments showed a gradual release of iron over time, reaching 0.04-0.05 g/m^2 by 100 days (Figure 6). However, the biotic LAWA44 glass showed initially high iron release at 2 days (0.46 g/m^2) but decreased over time until reaching 0.07 g/m^2 at 100 days, which is similar to the other three glasses. There was very low iron release in all four abiotic glass treatments, with the greatest release measured in the LAWA44 glass at 49

days (0.011 g/m^2). For sodium, the abiotic and biotic trends for the Join(mid), Join, and LAWA44 glasses mimicked the boron release (Figure 7). Both biotic and abiotic Dark glasses showed a negative sodium release at earlier time points (2-49 days), indicating removal of sodium from the solution, most likely from uptake into the *Paenibacillus* biomass [58]. After 100 days, the release of sodium from biotic and abiotic Dark glass reached 0.28 g/m^2 and 0.06 g/m^2, respectively. For silicon, the biotic glass trends mirrored the iron release and achieved approximately the same level of elemental release, 0.04-0.07 g/m^2 for iron and 0.05-0.06 g/m^2 for silicon (Figure 8). All abiotic glasses released 0.03 g/m^2 of silicon after 100 days. The greatest difference in elemental release between the biotic and abiotic glasses was seen in the Join glass, while the Dark glass and Join(mid) glasses showed only slightly greater release for the biotic glass compared to the abiotic glass.

Table 9. Normalized release of selected elements in samples tested in depleted HOD at 100 days. Note: Dark glass composition does not contain boron.

	Normalized release (g/m^2) at 100 days							
	Dark glass		Join(mid) glass		Join glass		LAWA44 glass	
Element	**Biotic**	**Abiotic**	**Biotic**	**Abiotic**	**Biotic**	**Abiotic**	**Biotic**	**Abiotic**
Boron (B)	Not present	Not present	0.16*	0.07*	2.12 ± 0.144	0.72*	0.59 ± 0.006	0.09*
Iron (Fe)	0.04 ± 0.000	0.00 ± 0.000	0.05*	0.00*	0.05 ± 0.015	0.00*	0.07 ± 0.000	0.00*
Sodium (Na)	0.28 ± 0.100	0.06 ± 0.147	0.20*	0.15*	1.68 ± 0.113	0.58*	0.84 ± 0.002	0.24*
Silicon (Si)	0.05 ± 0.001	0.03 ± 0.004	0.06*	0.03*	0.06 ± 0.002	0.03*	0.06 ± 0.001	0.03*

Values are single replicates (*) or averages of duplicate samples with ± standard deviations.

VZPW-amended. By 100 days in the VZPW-amended treatments, the biotic and abiotic Join glass had the greatest overall elemental release, followed by the LAWA44 glass, and Join(mid) glass (Table 10). Release from the biotic Join and LAWA44 glasses was greater than the corresponding abiotic glasses for all elements. However, the biotic Join(mid) glass showed comparable or only slightly greater release than the abiotic Join(mid) glass for all elements of interest. For boron, the biotic Join glass reached an order of magnitude greater release than the biotic Join(mid) and LAWA44 glasses at 100 days (Figure 5). The abiotic Join glass released four times more boron (0.27 g/m^2) after 100 days compared to the Join(mid) and LAWA44 glasses, which reached 0.08 g/m^2 for both glasses. Release of iron from biotic and abiotic Join(mid) and Join glasses followed very similar trends from 2 to 100 days (Figure 6). However, while the abiotic LAWA44 glass saw similar release to the other abiotic glasses, release of iron from biotic LAWA44 glass increased at 7 days (0.18 g/m^2) and 14 days (0.23 g/m^2) but decreased to 0.03 g/m^2 by 100 days, which was comparable to the biotic Join(mid) and Join glasses at 100 days. For sodium (Figure 7), the trends were similar to the boron release for biotic and abiotic Join(mid) and LAWA44 glasses, where the sodium release was slightly greater than the boron release (Figure 5). While the general sodium trend with time was similar to the boron trend for the biotic and abiotic Join glass, there was greater boron release than sodium for the biotic Join glass, in contrast with the other two biotic glasses. The silicon release (Figure 8) from the abiotic and biotic Join(mid) and LAWA44 glasses and abiotic Join glass was similar to the iron release with time and magnitude at 100 days. However, the biotic LAWA44 glass had increased iron and silicon release at 7 days and 14 days, followed by a decrease in release from 28 to 100 days. In contrast to the other glasses, the biotic Join glass had two times greater iron release than silicon release at 100 days.

The VZPW-amended tests also included a static set of abiotic and biotic LAWA44 glass samples to evaluate the impact of tumbling on the release rates (Table 11). In general, the biotic glass, tumbled and static, had greater elemental release than the corresponding abiotic glass for all elements. The release

rates for the abiotic glass were approximately the same, regardless of tumbling. The differences in normalized release for the biotic tumbled vs biotic static LAWA44 glasses were element dependent. At 100 days, boron and sodium had greater release when tumbled (Figures 6 and 8), silicon reached the same release (Figure 8), and iron saw two times greater release in the static vs the tumbled (0.07 g/m^2 vs 0.03 g/m^2, respectively) (Figure 6). Another difference was the lower elemental release of all the elements of interest from the biotic static glass from 2 to 28 days, which gradually increased to become more similar to the biotic tumbled release from 28 to 100 days.

Table 10. Normalized release of selected elements in samples tested in VZPW-amended at 100 days. Note: Dark glass was not tested in this medium, and LAWA44 glass values are for tumbled solutions.

	Normalized release (g/m^2) at 100 days							
	Dark glass		**Join(mid) glass**		**Join glass**		**LAWA44 glass**	
Element	**Biotic**	**Abiotic**	**Biotic**	**Abiotic**	**Biotic**	**Abiotic**	**Biotic**	**Abiotic**
Boron (B)	Not tested	Not tested	0.08 ± 0.002	0.08 ± 0.000	1.64 ± 0.006	0.27 ± 0.004	0.51 ± 0.011	0.08*
Iron (Fe)	Not tested	Not tested	0.01 ± 0.001	0.00 ± 0.001	0.04 ± 0.003	0.00 ± 0.000	0.03 ± 0.006	0.01*
Sodium (Na)	Not tested	Not tested	0.14 ± 0.015	0.16 ± 0.008	1.21 ± 0.020	0.28 ± 0.007	0.74 ± 0.016	0.24*
Silicon (Si)	Not tested	Not tested	0.01 ± 0.000	0.01 ± 0.000	0.02 ± 0.001	0.00 ± 0.000	0.02 ± 0.000	0.01*

Values are single replicates (*) or averages of duplicate samples with ± standard deviations.

Table 11. Normalized release of selected elements in LAWA44 samples tested in VZPW-amended at 100 days for tumbled and static solutions.

	LAWA44 Normalized release (g/m^2) at 100 days			
	Tumbled		**Static**	
Element	**Biotic**	**Abiotic**	**Biotic**	**Abiotic**
Boron (B)	0.51 ± 0.011	0.08*	0.45 ± 0.019	0.03 ± 0.001
Iron (Fe)	0.03 ± 0.006	0.01*	0.07 ± 0.007	0.00 ± 0.001
Sodium (Na)	0.74 ± 0.016	0.24*	0.64 ± 0.023	0.19 ± 0.000
Silicon (Si)	0.02 ± 0.000	0.01*	0.02 ± 0.000	0.00 ± 0.001

Values are single replicates (*) or averages of duplicate samples with ± standard deviations.

Discussion

Abiotic glass dissolution occurs due to the breakdown of the silicate network through chemical interaction with the surrounding aqueous solution. Glass dissolution kinetics are influenced by variables such as glass composition, pH, temperature, and solution composition [59, 60]. The release of soluble elements from the glass into the surrounding environment alters the surface chemistry and structure through the formation of alteration layers that ultimately slow glass dissolution. These stages of glass dissolution are well documented for nuclear waste glass, as long-term chemical durability and the potential for radionuclide release must be determined from a safety standpoint [5, 61, 62].

In these abiotic experiments, elemental release into solution followed the expected trends for glass dissolution. Silicon (Si) is the primary network forming element in glass and creates Si–O–Si linkages. Dissolution of the Si–O bond is primarily driven via hydrolysis, where water attacks the Si–O–Si bonds in the matrix [63], which breaks down the glass structure and releases silicic acid into solution. Because silicic acid is retained in the alteration layer, it is released more slowly than sodium (Na). Na^+ modifies the glass network, as it disrupts the primary silicate linkages. It can undergo diffusion-driven ion exchange with hydrogen (H^+) or hydronium (H_3O^+) ions, prior to silicate bond breakage [13]. Boron (B) is a network former [64-67] but has complex behavior depending on the glass composition. Exchange of H^+ for Na^+ bonded to BO_4 tetrahedra results in hydrolysis [68], meaning that B is more readily released into solution than Si, which makes it a useful tracer for glass alteration [69]. Iron (Fe) can substitute into the silicate network and is present as Fe(II) or Fe(III) in tetrahedral or octahedral coordination. Upon leaching from glass under oxic conditions, any Fe(II) will rapidly oxidize to Fe(III), precipitate as secondary phases on the glass surface, and the concentration in solution remains low. Various organic compounds are also known to interact with iron, or other trivalent cations via ligands, chelators, and siderophores. These organic interactions often increase biological alteration of iron rich glasses (e.g., basaltic glass) due to the metabolic needs of iron either as an enzymatic cofactor or for cellular respiration [70, 71], however ferrous iron is less likely to be oxidized directly from microbial interaction [72]. The different aqueous chemistry did affect elemental release in the abiotic experiments. Join glass released more Si and Fe in DIW than in depleted HOD. The pH for all glass compositions in DIW increased over time, consistent with exchange of H^+ for alkali and alkaline earth ions (e.g., Na^+, K^+, Ca^{2+}, and Mg^{2+}), which are released into solution [13]. Glass composition also had an effect, with the two join glasses releasing more B into solution than LAWA44, due to the greater fraction of alkali and alkaline earth elements.

However, these abiotic processes alone cannot be used to predict glass dissolution rates in natural environments, suggesting a role for other environmental factors, including microbial activity [16, 73-77]. Microorganisms can enhance glass dissolution through a variety of mechanisms, including the production of organic acids, siderophores, extracellular polymeric substances (EPS), and redox active metabolites that can destabilize lattice structures via dissolution or chelating metal ions [78, 79]. Biofilm formation can also increase internal transport of nutrients and waste through channels and structural features but can also decrease external mass transfer with the surrounding environment [80].

Microbial activity can be represented by an increase in cell density. In depleted HOD solutions with key elements for growth (Fe, Mn, B, and Mo) removed from the medium, the cell densities were greater in the presence of glass than in the absences of glass. This suggests that the microbes were able to access these essential nutrients from the glass to promote cell growth [81, 82]. This trend is also seen for Join(mid) glass in VZPW-amended, but the cell density was the same in the presence or absence of Join and LAWA44, suggesting that the interplay between glass composition and solution chemistry has a significant effect on cell growth. While the overall release of elements from glass in depleted HOD was greater, cell growth was higher in VZPW-amended. This suggests that planktonic cell density is not the only driver of glass dissolution, and that cellular stress can also play a role. The cells in depleted HOD may have been under greater stress, due to the lower buffering capacity at lower pH, and their stress response, including accumulation of cellular products, EPS, and sporulation, could accelerate glass

dissolution [83, 84]. Cell density trends with time also highlight the importance of extended tests to understand microbial behavior. Over the first 2 days, when nutrients (e.g., carbon source, nitrogen, casamino acids) were readily available, cell density increased rapidly corresponding to exponential growth. Over longer time periods (> 49 days), the cells were nutrient limited, with growth slowing to a stationary phase that was sustained by periodic nutrient spiking.

Cell association with the glass was qualitatively evaluated using CLSM imaging. In both depleted HOD and VZPW-amended, CLSM images for Dark, Join(mid), and Join glass showed individual *Paenibacillus* cells, mostly located between the glass particles. For LAWA44 glass, *Paenibacillus* cells were also mostly interstitial, but were primarily observed in clusters rather than as individual cells. This "swarming" behavior is characteristic of *Paenibacillus* cells and could be an environmental stress response to the presence of toxic heavy metals (e.g., chromium, lead) in the LAWA44 glass [44]. A washing step with the corresponding media removed most of the cells, indicating that the cells did not strongly adhere to the glass as a biofilm, but were likely planktonic cells in solution. CLSM images for Join glass exposed to *Paenibacillus* cells in both depleted HOD and VZPW-amended, revealed the formation of fluorescent euhedral octahedral crystals that were not present in any other glass sample, biotic or abiotic. Powder x-ray diffraction (XRD) patterns for these Join glass samples (Figure S3) showed peaks corresponding to quartz that were not present in the patterns for the other glass samples. Quartz crystallization from supersaturated aqueous solutions has been demonstrated at room temperature over hundreds of days [85]. It is possible that the constant tumbling of silica-rich glass suspensions in the presence of microbes in these experiments accelerated quartz precipitation. The crystals in SI Figure S3 exhibit auto fluorescence, which is not expected for pure quartz, but could be due to the incorporation of impurities. Formation of calcium oxalate from reaction between the calcium in solution and oxalate from microbial metabolism could have occurred in these experiments. Calcium oxalate exhibits autofluorescence when excited by ultraviolet light, which may explain the fluorescent crystals, but there are no reflections corresponding to calcium oxalate in any of the XRD patterns.

Results show that pH plays a key role in the microbially-induced glass dissolution. HEPES buffer was added to the initial solutions to maintain the pH at 7.0 for depleted HOD and at 7.9 for VZPW-amended. VZPW-amended also contains bicarbonate, so it has additional buffering capacity. However, *Paenibacillus* cells were able to overcome the buffering capacity and, in most cases, reduced the pH to ≤ 5.7 through the production of organic acids [86]. This reduction in pH increased glass dissolution, as confirmed by the increased concentration of dissolved ions in solution. As shown in the abiotic experiments, the presence of glass has the opposite effect and increases pH through ion exchange. Therefore, when both glass and *Paenibacillus* cells are present, the relatively stable pH indicates a balance between microbial activity acidifying the solutions, and glass dissolution increasing pH. Cell growth over time is also impacted by changes in pH due to formation of metabolic products, such as organic acids, which accumulate over time [87, 88]. While progressive glass dissolution in the presence of organic acids increases the concentration of ions in solution, the accumulation of metabolic and waste products creates an increasingly hostile environment for microbes. As the cells react to this dynamic environment, they begin to use alternative metabolic processes, as described below.

Glass dissolution was greater in biotic samples than in their abiotic counterparts, likely due to production of organic acids, as shown by NMR. Organic acids can interact with glasses in various ways, such as ion exchange and metal-acid complexation. Ion exchange was apparent with the Join glass, as H^+ in the solution replaced the alkali/alkaline earth metals on the glass surface, resulting in a large increase in Na and B in solution. Organic acids, specifically those with active functional groups (e.g., carboxyl groups (–COOH)), can strongly complex with the metal ions, further extracting those elements. Carboxylic acids, such as formic (HCOOH), acetic (CH_3COOH), and dicarboxylic acids (e.g., oxalic and meso-oxalic), are particularly aggressive as they form stable complexes with boron. While the NMR analysis did not highlight any significant increases in dicarboxylic acids, various other common organic acid compounds were identified, most notably acetic, formic, butyric, and lactic acids. These analytes highlight multiple

branches of pyruvate metabolism [89] and align with known capabilities in *Paenibacillus* spp. for mixed-acid fermentation [54]. These findings suggest the use of diverse pyruvate pathways to maintain energy yields and redox balance (e.g., pH buffering through the release of reactive oxygen and nitrogen species) under anaerobic conditions, which could develop in between the weekly tube "venting" that was intended to keep the conditions aerobic. In the absence of glass, there was increased glucose consumption, increased acetate production, and reduced net lactate production, suggesting variations in pyruvate metabolism, likely due to the lack of additional resources available to be scavenged. The NMR results showed that the presence of different glasses resulted in slightly different amino acid content, likely due to interactions between the supplemented casamino acids and the trace metals in solution [90].

The apparent shifts between alternative metabolic processes observed in the NMR data were likely motivated by changes in pH. For example, at neutral pH (~7), bacterial cells are known to grow exponentially, resulting in the production of acids, primarily lactate, acetate, and formate when glucose is abundant, but also hydrogen gas and carbonic acid [91]. At lower pH (< 6), acid accumulation begins to inhibit bacterial production of acidic products via a negative feedback loop [88], resulting in a change in production to acetoin, 2,3-butanediol, and ethanol [55]. NMR detection of both acidic and neutral metabolites over time, along with the lowered pH of the solutions past the buffering capabilities of HEPES and bicarbonate, suggests the adoption of a pH-dependent metabolic shift as a bacterial survival strategy. This is supported by the cell density data which generally increases throughout the experiment, or shows variations that can be accounted for by decreased microbial growth rate and/or increased sporulation as a result of changes in pH [92, 93]. Also, the amino acids glutamine and arginine were present, and their metabolism plays an important role in the ability of lactic acid fermenting bacteria to adapt to acidic environments [56]. These findings suggest that glasses exposed to *Paenibacillus* cells could be subjected to acidic environments and undergo selective ion leaching, in addition to silica network hydrolysis over time [94, 95].

Comparison of tumbling versus static tests for VZPW-amended solution with and without LAWA44 revealed that both the final cell density and the relative elemental release were impacted. In CLSM images, more cells were attached to LAWA44 in static tests compared to tumbled tests, indicating that shear forces during tumbling prevented cells from adhering to the glass surface. However, tumbling with and without glass did increase cell growth, likely due to better nutrient mixing and aeration [95]. This suggests that *Paenibacillus* cell growth was driven by nutrient availability, rather than by establishing biofilms on the glass. Microorganisms other than *Paenibacillus* may attach more strongly to the glass, even with tumbling, due to more aggressive biofilm generation. The elemental release rate from LAWA44 was different between the tumbled and static tests, with B and Na release beginning at ~7 days in the tumbled solutions, and at 14 or 28 days in static tests. However, overall release of B and Na (at 49 and 100 days) was similar in both tumbled and static tests, and was considerably higher in the presence of *Paenibacillus* cells than the corresponding abiotic tests. The similarities in overall release indicate that it is most likely driven by indirect biological processes, or that there were not enough cells in direct contact with the glass to have an observable impact on the elemental release trends. While additional glass compositions should be evaluated, these results show that the addition of *Paenibacillus* cells had the most impact on elemental release from LAWA44, whether the samples were tumbled or remained static.

In this study, we examined the influence of microbial processes on glass dissolution. We showed that the presence of *Paenibacillus* cells increased the rate of glass dissolution compared to the corresponding abiotic samples. This effect became more pronounced over time due to changes in aqueous chemistry, cell growth, and generation of metabolites. There is a dynamic relationship between the *Paenibacillus* cells and the glass, which is influenced by glass composition and solution chemistry. In the absence of *Paenibacillus* cells, the higher Na content (20 wt.%) Join glass was less chemically durable, as expected from previous studies [97]. Cell growth in depleted HOD with Join glass was also highest, resulting in more organic acid production, but this was counteracted by the increased glass dissolution, resulting in a higher pH and greater B and Na release over time. For more durable glasses with less than 15 wt% Na2O

(Dark, Join(mid), and LAWA44), production of organic acids by *Paenibacillus* cells reduced pH, resulting in lower B and Na releases. This suggests that elemental release from less durable glasses increases pH and compensates for microbially produced organic acids so that the pH remains circumneutral, providing a more favorable environment for microbes. This continued cycle would ultimately sustain microbial growth and lead to higher levels of B and Na release. This suggests that microbially-induced glass dissolution is in an indirect effect driven by the generation of organic acids and does not result from direct contact of *Paenibacillus* cells with the glass surface. These findings provide new insights into the influence of microbial processes on glass dissolution, and underscore the complexity of natural systems, which are governed not only by the metabolic activity of microorganisms, but also by the glass composition and the chemistry of the surrounding environment [73, 78, 98].

When considering the implication of these results for disposal of LAW glass in the IDF at Hanford, it is important to consider several factors in this study's experimental design. These tests supplied ample organic carbon (i.e., glucose) for the *Paenibacillus* cells, which accelerated and maintained biomass growth for the duration of the experiment. At Hanford, the subsurface is low in organic carbon, which will constrain the level of microbial activity. This study evaluated the influence of a single microorganism, whereas Hanford subsurface sustains a microbial community (i.e., bacteria, fungi, and archaea), which may interact with glass via different mechanisms than those studied here. This study demonstrated the importance of glass composition on microbial effects; therefore, more glass compositions in addition to the four tested here need to be evaluated. Future work will investigate the effect of unsaturated conditions and incorporate subsurface material that will be in contact with the glass, including the associated native microbial community, to provide a more complete biogeochemical evaluation of field conditions. The longer timescales in this study highlighted that results from a two-day dissolution test cannot easily be extrapolated to longer timeframes when the effect of microbes is included. Additional work is required to understand how to extrapolate results from lab-scale testing to predict the effect of microbial colonization on glass dissolution at field-scale.

Methods

Glass Preparation

Formulation. Four glass compositions were tested, 1) simulated "Dark" glass based on the Broborg hillfort mafic glass, 2) two 'join' glasses that bridge the composition of the Dark glass and low activity waste (LAW) glass, and 3) a composition representative of one of the LAW glass compositions that will be produced at the Hanford Waste Treatment and Immobilization Plant and disposed onsite in the IDF ("LAWA44"). The two join glasses were designed by modifying the Dark glass composition to include greater concentrations of boron and sodium [38]. The "Join" glass contains 10 wt% boron oxide (B_2O_3) and 20 wt% sodium oxide (Na_2O) (glass name D-10B-20N, where D=dark glass, B=boron, N=sodium), whereas the "Join(mid)" glass contains 6 wt% B_2O_3 and 10 wt% Na_2O (glass name D-6B-10N) [39]. Complete compositions in mass% are provided in Table 12. The molar ratio of the components B, Ca, Fe, Mg, and Na to Si are provided in Table S12.

Fabrication. Carbonate salts of alkali and alkaline earth metals, boric acid, sodium hexametaphosphate, sodium sulfate, sodium fluoride, sodium chloride, zirconium hydroxide, potassium perrhenate, and single metal oxides were weighed in the appropriate masses to form the target glass composition for each glass (Table 12). An Angstrom vibratory mill with an agate puck was used to mix the oxides for 1-2 minutes. The powdered oxide mixture was transferred to a clean platinum (Pt)/10% rhodium (Rh) crucible for melting using a multi-step melt process shown in Table 13 with specific melt times and temperatures for the glasses. Glass-forming melts were air quenched on an Inconel pour plate.

Quenched glasses were size reduced to powders using a tungsten carbide puck mill. The powders were then hand-sieved using a sieve tower of #100 and #200 to separate glass powder between 75 and 150 µm.

The glass powder is assumed to have a spherical geometry following the methodology applied by McGrail et al. [40]. This assumption results in a glass specific surface area of 0.02 m^2/g. The glass powders were then washed with deionized water (DIW) at 18.2 $M\Omega \cdot cm^{-1}$ followed by 70% ethanol to remove any remaining fines. After washing, the powders were placed in a drying oven at 90 °C for 4–12 hours.

Table 12. Glass compositions given in mass percentages.

	Target Mass Percent (%)			
Constituent	**Dark**	**Join(mid)**	**Join**	**LAWA44**
Al_2O_3	12.77	10.46	8.71	6.08
B_2O_3	0	6.00	10.00	10.06
CaO	8.73	7.42	6.18	5.12
Cl	0	0	0	0.09
Cr_2O_3	0	0	0	0.02
F	0	0	0	0.16
Fe_2O_3	12.83	10.84	9.03	5.43
K_2O	1.39	0.91	0.76	0.1
Li_2O	0	0	0	2.51
MgO	6.68	7.8	6.5	1.51
MnO	0.43	0.28	0.23	0.04
MoO_3	0	0.1	0.1	0
Na_2O	2.78	10	20	14.4
NiO	0	0	0	0.03
P_2O_5	0.2	0.16	0.13	0.17
PbO_2	0	0	0	0.02
Re_2O_7	0	0.1	0.1	0.01
SiO_2	53.68	45.33	37.76	46.67
SO_3	0	0	0	0.34
TiO_2	0.89	0.61	0.5	1.14
ZnO	0	0	0	3.07
ZrO_2	0	0	0	3.03

Table 13. Glass melt temperatures and times.

	Melt 1		Melt 2		Melt 3	
Glass	**Temp (°C)**	**Time (hr)**	**Temp (°C)**	**Time (hr)**	**Temp (°C)**	**Time (hr)**
Dark	1300	0.75	1415	0.25	Not needed	Not needed
Join(mid)	1200	0.5	1200	0.25	1200	0.75
Join	1100	0.25	1100	0.25	1130	0.75
LAWA44	1150	1.0	1150	1.0	Not needed	Not needed

Sterilization. Glass vials were autoclaved under standard conditions (15 psi and 121 °C), then 3 g (±0.0010 g) of glass powder was placed in each vial. Foil covers were used to prevent biological re-contamination. Vials with the powder were then placed in an oven at 90 °C (± 5 °C) for 3 hours and then transferred to a biological safety cabinet (BSC) to cool. Once cooled, the vials were stored in the dark at room temperature. The oven cycling was repeated for a total of three consecutive days to eliminate spore-forming microorganisms on the glass powders.

Solution Preparation

Test media. Two minimal growth media were used in these tests (see Table 14 for compositions). A hydrogen oxidizing denitrifier (HOD) medium was modified based on Lee et. al (2015) to exclude certain trace elements, referred to as "depleted HOD" herein [41]. This modification was made to encourage bacterial interactions with the glass and to lower background aqueous concentrations of elements present in the glass. The modification removed the American Type Culture Collection mineral supplement and instead added individual stocks of trace elements (Co, Zn, Cu, Se, W, Ni, Mg) and omitted trace elements present in the glass compositions (Fe, Mn, B, and Mo). While boron is not included in the Dark glass composition, boron was not added to any of the solutions as a trace element stock. A VZPW recipe was designed based on data from ongoing lysimeter studies [42] for the Hanford Site IDF to provide field-relevant chemistry for the solution in contact with disposed LAW glass. The inorganic VZPW recipe was then amended ("VZPW-amended") to include critical biological constituents (NH_4Cl, NaH_2PO_4, vitamins, and casamino acids) at the same concentrations as those used in the depleted HOD medium. Both the depleted HOD and VZPW-amended media used glucose (10 mM) as an electron donor and carbon source, with periodic additional glucose amendments for samples incubated for longer times (see "Solution preparation" section in Methods). The media were pH adjusted to 7.0 for depleted HOD and 7.9 for VZPW-amended and buffered using 4-(2-hydroxyethyl)piperazine-1-ethanesulfonic acid) (HEPES) at 30 mM and 15 mM for depleted HOD and VZPW-amended, respectively. HEPES buffer is known for its high solubility, lack of toxicity, and minimal interference in biological processes, and is also zwitterionic, making it resistant to pH changes. The VZPW-amended recipe also included sodium nitrate ($NaNO_3$) and bicarbonate ($NaHCO_3$), whereas the depleted HOD did not.

The glasses were also tested in deionized water (DIW) to mimic the EPA 1313 method and monitor the behavior of the glasses without the pH buffering capacity of the test media and without the influence of microbes.

Table 14. Compositions of test media for the depleted hydrogen oxidizing denitrifier, "depleted HOD," and bio-amended vadose zone porewater, "VZPW-amended."

	Depleted HOD	**VZPW-amended**
Base Compositions	**Concentration, mM (g/L)**	**Concentration, mM (g/L)**
$MgCl_2$	0.5 (0.048)	-----
KCl	0.2 (0.015)	-----
$CaCl_2 \cdot 2H_2O$	0.6 (0.088)	0.060 (0.009)
$CaSO_4 \cdot 2H_2O$	-----	0.300 (0.052)
$SiO_2 \cdot 2H_2O$	-----	0.491 (0.047)
$NaHCO_3$	-----	1.430 (0.120)
$Ca(NO_3)_2 \cdot 4H_2O$	-----	0.400 (0.094)
$MgSO_4$	-----	0.260 (0.031)
$KHCO_3$	-----	0.087 (0.009)
NH_4Cl	1.00 (0.054)	3.00 (0.160)
NaH_2PO_4	0.10 (0.012)	0.10 (0.012)
Glucose	10.0 (1.802)	10.0 (1.802)
HEPES	30 (7.149)	15 (3.575)
Wolfe's Vitamins	1x (10 mL/L)	1x (10 mL/L)
Casamino Acids	0.01%	0.01%
Trace Elements	**Concentration, µM (mg/L)**	**Concentration, µM (mg/L)**
$Co(NO_3)_2 \cdot 6H_2O$	3.440 (1.00)	3.440 (1.00)
$ZnSO_4 \cdot 7H_2O$	3.480 (1.00)	3.480 (1.00)
$CuSO_4 \cdot 5H_2O$	0.400 (0.100)	0.400 (0.100)
Na_2SeO_3 (anhydrous)	0.058 (0.010)	0.058 (0.010)
$Na_2WO_4 \cdot 2H_2O$	0.303 (0.100)	0.303 (0.100)
$NiCl_2 \cdot 6H_2O$	0.842 (0.200)	0.842 (0.200)
$MgSO_4 \cdot 7H_2O$	156.0 (38.4)	156.0 (38.4)
Target pH	7.0 ± 0.1	7.9 ± 0.1

Media supplementation. Once per week, all samples (except the DIW samples) were opened to the atmosphere (in the BSC) and supplemented with one of the following: glucose (5 mM), casamino acids (0.01%), or ammonium chloride (NH_4Cl, 1 mM), or were vented to refresh air. These supplements were added to sustain the bacterial culture for the duration of the experiments and were also added to the abiotic samples for consistency with the biotic samples.

Bacterial Strain

Selection. The microbe used is a *Paenibacillus* strain (strain name "300A") that was isolated from the subsurface of the 300 Area of the Hanford Site [37]. Strain 300A is a facultatively anaerobic Fe(III) reducer that readily forms biofilms [38], demonstrates swimming (tumbling) motility [43], and is closely related to *P. vortex* [40]. *Paenibacillus* species (formerly *Bacillus*) are Gram-positive, endospore-forming bacteria that are commonly motile via swarming behavior [44]. Members of the *Paenibacillus genus*, as well as members of the larger *Paenibacillaceae* family, were identified in the surface-exposed vitrified material at the Broborg hillfort site and the associated soil [30]. Likewise, *Paenibacillus* species have been recovered from the Hanford subsurface [37, 45]. *Paenibacilli* are common inhabitants of the plant rhizosphere, where they often function as plant growth promoting bacteria [46]. *Paenibacillus* species are

known to affect mineral weathering [31, 47-49], and to solubilize potassium (K^+) and phosphate (PO_4^{3-}) ions from minerals [50, 51]. In addition, *Paenibacilli* can form biofilms on glass surfaces [52].

Cultivation. Paenibacillus strain 300A was inoculated from a 20% glycerol freezer stock (-80 °C) onto agar plates of trypticase soy broth (TSB) medium, without dextrose. The plates were incubated at 30 °C, in the dark, until colonies were visible. Individual colonies were then transferred to 5 mL of liquid replete HOD medium (including ATCC vitamin and mineral supplements) with glucose (10 mM) and incubated at 30 °C in the dark, without shaking, until the cultures were turbid (~3 days), to provide the starter culture for the experiments.

Modified EPA 1313 Glass Corrosion Tests

Samples were tested in the following combinations: (i) solution, glass, and microbe; (ii) solution and glass; (iii) solution and microbe; (iv) solution only. The combinations of solutions and glasses tested are shown in Table 15. Note, additional sets of samples containing LAWA44 glass and no glass, with and without the microbe, were tested in the VZPW-amended solution under static (no tumbling) conditions to determine the extent to which tumbling would impact the elemental release from the glass and the behavior of the microbe.

Within a BSC, 30 mL of the solution (depleted HOD, VZPW-amended, or DIW), 3 g of glass, and 300A starter culture (6%, volume/volume) were added to the appropriate 50 mL centrifuge tubes (VWR, polypropylene) (Figure 9). The ratio of glass surface area to volume was 2,100 m^{-1}. All work within the BSC included use of 70% ethanol to wipe down BSC surfaces and pipets to maintain aseptic conditions. Samples were tumbled end-over-end at 30 rpm at room temperature, in the dark, for the duration of the experiment (Table 15). End-over-end tumbling, which is a requirement of EPA Method 1313, also ensured homogeneous solution mixing. Solution subsampling for ICP-OES was performed on 2, 7, 14, 28, 49, 100, and 200 days. Samples were terminated on 2, 49, and 100 or 200 days. At these termination points, liquid samples were measured for pH and optical density at 600 nm and subsamples were saved for ICP-OES, NMR, and total organic carbon. The glass powders were also collected for CLSM. Final solution volumes for each sample were kept within 10% of the original solution volume.

Table 15. Testing matrix of glasses and solutions with corresponding test duration. Numbers in parentheses are the number of experimental replicates present at experiment initiation.

Glass	DIW	Depleted HOD	VZPW-amended
Dark	200 days (2)	200 days (2)	Not tested
Join(mid)	100 days (1)	100 days (2)	100 days (2)
Join	200 days (4)	200 days (4)	100 days (4)
LAWA44 – Tumbled	200 days (2)	100 days (2)	100 days (4)
LAWA44 – Static	Not tested	Not tested	100 days (2)
No glass – Biotic	Not tested	200 days (4)	100 days (4)
No glass – Abiotic	200 days (4)	200 days (4)	100 days (4)

pH, Optical Density

Sample pH was measured by a Thermo Scientific™ Orion™ VersaStar Pro benchtop meter with an Orion™ ROSS Ultra pH/ATC triode. The meter was calibrated with commercial pH buffers at pH 4, 7, and 10 before each use. A separate set of commercial pH buffers from a different manufacturer were used to confirm successful calibration before and after sample measurements. Samples were filtered with a 0.2-µm H-PTFE syringe filter to remove any suspended bacterial cells or fine glass particles prior to pH measurement.

Optical density measurements were taken at 600 nm with an Orion AquaMate 8000 spectrophotometer (Thermo Fisher, Waltham, MA). The instrument was blanked with fresh, unreacted solution (depleted HOD or VZPW-amended, accordingly). Aliquots were taken from the original sample tubes 5 minutes after removing the samples from the tumbler. This was enough time for the glass particles to settle to the bottom while the bacterial cells stayed suspended in the solution. The solution aliquots were diluted in corresponding sterile medium and added to disposable poly(methyl methacrylate) 12.5 mm cuvettes. The values from the spectrophotometer are reported here as a dimensionless arbitrary unit.

Inductively Coupled Plasma-Optical Emission Spectroscopy (ICP-OES)

Each solution sample was taken 5 minutes post-tumbling (as done in the optical density measurements), diluted by 10x with 2% nitric acid (VZPW-amended samples) or 2% hydrochloric acid (depleted HOD samples), and filtered with a 0.2-µm hydrophilic polytetrafluoroethylene syringe filter. Samples were stored at 4 °C in the dark until ICP-OES analysis was performed. The eluate concentration of inorganic major species (e.g., B, Na, Si, etc.) was determined following EPA Method 6010D on an Agilent 5110 ICP-OES (Agilent Technologies, Santa Clara, CA). Five-point standard curves were used for an analytical range between approximately 25 and 25,000 µg/L. A seven-point standard curve for selected species was used for a lower limit of quantification (LLoQ) of 25 µg/L and method detection limit (MDL) of less than 10 µg/L. Calibration check standards were included at approximately 500 µg/L. An internal reference standard of yttrium was used and a recovery within 15% of the specified concentration was required. Matrix blanks were measured every 10 to 20 samples and matrix spikes were measured every 10 samples, with the requirement that check standards matrix spikes were within 15% of the specified value and blanks were below quantification limits.

The ICP-OES results were used to calculate the normalized elemental release using the method from ASTM method C1285-14:

$$NL_i = \frac{c_i - c_{i,blank}}{f_i \times (S/V)} \qquad \text{Equation (1)}$$

Where NL_i, is the normalized elemental release of element i (g/m^2), c_i is the content of element i in solution (g/L), $c_{i,blank}$ is the concentration of element i in the blank solution (g/L), f_i is the mass fraction of element i in the sample prior to chemical alteration, and S/V is the surface area-to-volume ratio (m^{-1}) of the powders in the leachate solution.

Nuclear Magnetic Resonance (NMR)

Aliquots of unfiltered sample supernatant were stored at -80 °C prior to proton NMR analysis. After thawing, depleted HOD and VZPW-amended samples were diluted by 10% with the addition of an internal standard (5 mM 2,2-dimethyl-2-silapentane-5-sulfonate-d6 -NIST certified concentration) to aid quantification. All NMR spectra were collected using an 800 MHz Bruker Avance Neo with a TCl 800/54 H&F/C/N-D-05 Z XT cryoProbe. The 1D 1H spectra were collected following standard Chenomx data collection guidelines, employing a 1D NOESY pre-saturation experiment (noesypr1d) with 65536 complex points and 2048 scans at 298 K. The NOESY mixing time was 100 ms and the acquisition time was 4 s followed by a relaxation delay of 1.5 s, during which pre-saturation of the water signal was applied. Time domain free induction decays (72,114 total points) were zero filled to 131,072 total points before Fourier transform, followed by exponential multiplication (0.3 Hz line-broadening) and semi-automatic multipoint smooth segments baseline correction. Chemical shifts were referenced to the 1H methyl or 13C signal in DSS-d6 at 0 ppm. The 1D 1H-NMR spectra of all samples were processed, assigned, and analyzed using Chenomx NMR suite 9.2 with quantification of spectral intensities of compounds in the Chenomx library relative to the internal standard. Candidate metabolites present in each of the complex mixtures were determined by matching chemical shift, J-coupling, and intensity information of the experimental signals against signals of the standard metabolites in the Chenomx library. Signal to noise ratios (S/N) were measured using MestReNova (v.14.2.014) with the limits of

quantification and detection equal to an S/N of 10 and 3, respectively. Standard 2D experiments, such as 1H/13C - heteronuclear correlation (HSQC) or 2D 1H/1H -Total Correlation spectroscopy (TOCSY), further aided corroboration of several metabolite identifications where there was sufficient S/N.

Dissolved Organic Carbon (DOC)

Dissolved organic carbon (DOC) was analyzed on a Total Organic Carbon Analyzer (TOC-LCSH, Shimadzu Scientific Instruments, Columbia, MD, USA), a high temperature catalytic combustion analyzer equipped with a non-dispersive infrared detector for CO_2 quantification. Prior to analysis, samples were diluted, filtered through a 0.2 μm filter, and stored in a refrigerator (4 °C) until analysis. For DOC measurements, inorganic carbon was removed by acidifying samples with HCl to eliminate dissolved CO_2 and any carbonate species. Samples were loaded into the system and injected via autosampler with a sample injection of 100 μL. In the high temperature combustion furnace, organic carbon was oxidized to CO_2 in the presence of a platinum catalyst in an oxygenated environment, which was then quantified. Calibration of the instrument was performed using a multipoint calibration using certified potassium hydrogen phthalate standards.

Confocal Laser Scanning Microscopy (CLSM)

Samples in the original sample tubes, containing the solution and glass, were stained with SybrGold Nucleic Acid Gel Stain kit (Invitrogen, Carlsbad CA) by adding 1 μL of concentrated stain for every 10 mL of solution. After waiting 1 minute for the stain to diffuse throughout the solution, a small subsample of glass powder was removed from the original tube and placed onto a glass slide, where the powder was spread out to achieve an even layer on the slide. Two by two stitched confocal Z-stack microscope images of the SybrGold-stained powder samples were acquired at 1 μm z-steps on a Zeiss LSM 710 scanning head confocal microscope with a Zeiss LD C-Apochromat 40X/1.1 objective. The 488 nm excitation laser was used to excite the stain, and the emission signal was collected at 493 – 598 nm. Transmitted light images were collected simultaneously for each set of images. Laser dwell times were 0.79 ms. After collecting the images, the glass powder was transferred to a tube with fresh depleted HOD or VZPW-amended solution and allowed to sit for 3 minutes. This “wash” step would dislodge any biofilm only loosely associated with the powders. The powder was transferred from the wash tube back to a clean glass slide for imaging.

Powder X-Ray Diffraction (pXRD)

Glass samples were analyzed by XRD to identify the octahedral crystals that formed in some biotic samples. The glass was crushed into fine powder using a mortar and pestle and corundum (Al_2O_3) was added as an internal standard. Diffraction data were collected using a Rigaku MiniFlex II Bragg–Brentano diffractometer with Cu-Kα radiation (λ = 1.5418 Å) and a graphite post-diffraction monochromator. The Miniflex was operated at 30 kV and 15 mA and patterns were collected between 3 and 90 °2θ, using a scan width of 0.04° and a 5-second count time. Identification of material phases was carried out using JADE XRD pattern processing software and reference patterns from the International Centre for Diffraction Data powder diffraction database.

Acknowledgements

This work is supported by the Waste Treatment and Immobilization Plant Project at the United States Department of Energy (US DOE) Hanford Field Office (HFO). This study is also supported in part by the US DOE, under Cooperative Agreement Number DE-FC01-06EW07053 entitled ‘The Consortium for Risk Evaluation with Stakeholder Participation III’ awarded to Vanderbilt University. A portion of the research was performed using the Environmental Molecular Sciences Laboratory (EMSL), a national scientific user facility, sponsored by the DOE’s Office of Biological and Environmental Research, located at Pacific Northwest National Laboratory under proposal number 60748. Pacific Northwest National

Laboratory is operated for the US DOE by Battelle Memorial Institute under Contract DE-AC06–76RLO 1830. Graduate Fellow, A.R. Kennedy, was supported by the US DOE Office of Environmental Management – Minority Serving Institutions Partnership Program (EM MSIPP). We also thank Haluk Beyenal at Washington State University, Pullman, for providing *Paenibacillus* strain 300A.

Declarations

Author contributions. J.R.H., A.J.K., and A.R.K. wrote the main manuscript text and prepared all figures. All authors reviewed the manuscript. J.R.H., A.J.K., A.R.K., A.E.P., J.M., R.M.A., W.C., D.W.H., T.E.W., R.P.Y., T.W.W., R.C.D., and L.R.B. performed experimental work or data collection and analysis. J.R.H., A.J.K., A.E.P., W.C., D.W.H, R.P.Y., D.S.K., C.L.T., J.J.N., and C.I.P. contributed to the conceptualization of the experiments and methods development. J.J.N. and C.I.P. provided supervision and project administration. A.A.K. provided funding to support this work.

Competing interests. All authors declare no financial or non-financial competing interests.

Data availability

All data are available in the manuscript and supplementary information file or can be obtained from the corresponding authors upon request.

References

1. Scholze, H., *Nature and Structure of Glass*, in *Glass: Nature, Structure, and Properties*, H. Scholze, Editor. 1991, Springer New York: New York, NY. p. 3–155.
2. Karmakar, B., *Fundamentals of Glass and Glass Nanocomposites*. 2016. p. 3–53.
3. Chopinet, M.-H., *The History of Glass*, in *Springer Handbook of Glass*, J.D. Musgraves, J. Hu, and L. Calvez, Editors. 2019, Springer International Publishing: Cham. p. 1–47.
4. Axinte, E., *Glasses as engineering materials: A review.* Materials & Design, 2011. **32**(4): p. 1717–1732.
5. Marcial, J., et al., *Hanford low-activity waste vitrification: A review.* Journal of Hazardous Materials, 2024. **461**: p. 132437.
6. Peterson, R.A., et al., *Review of the Scientific Understanding of Radioactive Waste at the U.S. DOE Hanford Site.* Environmental Science & Technology, 2018. **52**(2): p. 381–396.
7. Zanini, R., et al., *A review of glass corrosion: the unique contribution of studying ancient glass to validate glass alteration models.* npj Materials Degradation, 2023. **7**(1): p. 38.
8. Frankel, G.S., et al., *A comparative review of the aqueous corrosion of glasses, crystalline ceramics, and metals.* npj Materials Degradation, 2018. **2**(1): p. 15.
9. Hench, L.L., *CHARACTERIZATION OF GLASS CORROSION AND DURABILITY*, in *Glass Surfaces*, D.E. Day, Editor. 1975, Elsevier. p. 27–39.
10. Lanford, W.A., et al., *Hydration of soda-lime glass.* Journal of Non-Crystalline Solids, 1979. **33**(2): p. 249–266.
11. Beall, G.H., et al., *Ion-Exchange in Glass-Ceramics.* Frontiers in Materials, 2016. **3**.
12. Gin, S., P. Dillmann, and N. Birbilis, *Material degradation foreseen in the very long term: the case of glasses and ferrous metals.* npj Materials Degradation, 2017. **1**(1): p. 10.
13. Gin, S., et al., *Aqueous alteration of silicate glass: state of knowledge and perspectives.* npj Materials Degradation, 2021. **5**(1): p. 42.
14. Addassi, M., H. Hoteit, and E.H. Oelkers, *The impact of secondary silicate mineral precipitation kinetics on CO2 mineral storage.* International Journal of Greenhouse Gas Control, 2024. **131**: p. 104020.

15. Sorint, S.S. and L.P. Jackson, *Evaluation of the toxicity characteristic leaching procedure (TCLP) on utility wastes.* Nuclear and Chemical Waste Management, 1988. **8**(3): p. 217–223.
16. Weaver, J.L., et al., *Microbial interactions with silicate glasses.* npj Materials Degradation, 2021. **5**(1): p. 11.
17. Barker, W.W., S.A. Welch, and J.F. Banfield, *Biogeochemical weathering of silicate minerals.* Reviews in Mineralogy and Geochemistry, 1997. **35**(1): p. 391–428.
18. Cockell, C.S., et al., *Alteration textures in terrestrial volcanic glass and the associated bacterial community.* Geobiology, 2009. **7**(1): p. 50–65.
19. Sharma, S., et al., *Microbial Biofilm: A Review on Formation, Infection, Antibiotic Resistance, Control Measures, and Innovative Treatment.* Microorganisms, 2023. **11**(6).
20. Flemming, H.-C., et al., *Biofilms: an emergent form of bacterial life.* Nature Reviews Microbiology, 2016. **14**(9): p. 563–575.
21. Konopka, A., et al., *Environmental controls on the activity of aquifer microbial communities in the 300 area of the Hanford site.* Microb Ecol, 2013. **66**(4): p. 889–96.
22. Bagnoud, A., et al., *Reconstructing a hydrogen-driven microbial metabolic network in Opalinus Clay rock.* Nature Communications, 2016. **7**(1): p. 12770.
23. Bell, E., et al., *Biogeochemical Cycling by a Low-Diversity Microbial Community in Deep Groundwater.* Frontiers in Microbiology, 2018. **9**.
24. Weber, K.A., L.A. Achenbach, and J.D. Coates, *Microorganisms pumping iron: anaerobic microbial iron oxidation and reduction.* Nat Rev Microbiol, 2006. **4**(10): p. 752–64.
25. Thorpe, C.L., et al., *Microbial interactions with phosphorus containing glasses representative of vitrified radioactive waste.* Journal of Hazardous Materials, 2024. **462**: p. 132667.
26. André, A.C., L. Debande, and B.S. Marteyn, *The selective advantage of facultative anaerobes relies on their unique ability to cope with changing oxygen levels during infection.* Cellular Microbiology, 2021. **23**(8): p. e13338.
27. Amundson, K.K., M.A. Borton, and M.J. Wilkins, *Anthropogenic impacts on the terrestrial subsurface biosphere.* Nat Rev Microbiol, 2025. **23**(3): p. 147–161.
28. Libourel, G., et al., *The use of natural and archeological analogues for understanding the long-term behavior of nuclear glasses.* Comptes Rendus Geoscience, 2011. **343**(2): p. 237–245.
29. Matthews, B.E., et al., *Micro- and Nanoscale Surface Analysis of Late Iron Age Glass from Broborg, a Vitrified Swedish Hillfort.* Microscopy and Microanalysis, 2023. **29**(1): p. 50–68.
30. Plymale, A.E., et al., *Niche Partitioning of Microbial Communities at an Ancient Vitrified Hillfort: Implications for Vitrified Radioactive Waste Disposal.* Geomicrobiology Journal, 2021. **38**(1): p. 36–56.
31. Parker, G.D., et al., *Molecular Imaging of Microbially Induced Corrosion of Synthetic Archeological Glasses by a Rhizosphere Bacterium.* Analytical Chemistry, 2025. **97**(26): p. 13872–13880.
32. Weaver, J.L., et al., *Pre-Viking Swedish hillfort glass: A prospective long-term alteration analogue for vitrified nuclear waste.* International Journal of Applied Glass Science, 2018. **9**(4): p. 540–554.
33. Choi, S., et al., *Application of pH-dependent environmental protection agency test method 1313 to low-activity nuclear waste glass.* Journal of Nuclear Materials, 2025. **614**: p. 155858.
34. Valbi, V., et al., *Bacterial diversity on stained glass windows.* International Biodeterioration & Biodegradation, 2023. **177**: p. 105529.
35. Verney-Carron, A., et al., *Alteration of medieval stained glass windows in atmospheric medium: review and simplified alteration model.* npj Materials Degradation, 2023. **7**(1).
36. Sterpenich, J. and G. Libourel, *Using stained glass windows to understand the durability of toxic waste matrices.* Chemical Geology, 2001. **174**(1): p. 181–193.
37. Ahmed, B., et al., *Fe(III) Reduction and U(VI) Immobilization by Paenibacillus sp. Strain 300A, Isolated from Hanford 300A Subsurface Sediments.* Applied and Environmental Microbiology, 2012. **78**(22): p. 8001–8009.

38. Marcial, J., et al., *Evaluating an EPA leaching test (Method 1313) to relate the long-term performance of nuclear waste glasses and ancient glasses*, in *Waste Management*. 2021: Phoenix, AZ, USA.
39. Marcial, J., et al., *Chemical durability assessment of enhanced low-activity waste glasses through EPA method 1313*. 2023, Pacific Northwest National Laboratory: Richland, WA, USA. p. 102.
40. McGrail, B.P., et al., *Measurement of kinetic rate law parameters on a Na-Ca-Al borosilicate glass for low-activity waste.* Journal of Nuclear Materials, 1997. **249**(2): p. 175–189.
41. Lee, J.-H., et al., *An autotrophic H2-oxidizing, nitrate-respiring, Tc(VII)-reducing Acidovorax sp. isolated from a subsurface oxic-anoxic transition zone.* Environmental Microbiology Reports, 2015. **7**(3): p. 395–403.
42. Bacon, D.H., et al., *Field-Scale Lysimeter Studies of Low-Activity Waste Form Degradation*. 2018: United States.
43. Berghouse, M., et al., *Advection-dominated transport dynamics of pili and flagella-mediated motile bacteria in porous media.* Soft Matter, 2025. **21**(18): p. 3622–3637.
44. Ingham, C.J., et al., *Mutually facilitated dispersal between the nonmotile fungus Aspergillus fumigatus and the swarming bacterium Paenibacillus vortex.* Proc Natl Acad Sci U S A, 2011. **108**(49): p. 19731–6.
45. Lee, J.-H., et al., *Microbial Reductive Transformation of Phyllosilicate Fe(III) and U(VI) in Fluvial Subsurface Sediments.* Environmental Science & Technology, 2012. **46**(7): p. 3721–3730.
46. Grady, E.N., et al., *Current knowledge and perspectives of Paenibacillus: a review.* Microbial Cell Factories, 2016. **15**(1): p. 203.
47. Wang, Y.L., et al., *Isolation and characterization of mineral-dissolving bacteria from different levels of altered mica schist surfaces and the adjacent soil.* World Journal of Microbiology and Biotechnology, 2018. **35**(1): p. 2.
48. Deo, N. and K.A. Natarajan, *Studies on interaction of Paenibacillus polymyxa with iron ore minerals in relation to beneficiation.* International Journal of Mineral Processing, 1998. **55**(1): p. 41–60.
49. Parker, G.D., et al., *Studying microbially induced corrosion on glass using ToF-SIMS.* Biointerphases, 2024. **19**(5): p. 051004.
50. Liu, D., B. Lian, and H. Dong, *Isolation of Paenibacillus sp. and Assessment of its Potential for Enhancing Mineral Weathering.* Geomicrobiology Journal, 2012. **29**(5): p. 413–421.
51. Qi, Y., et al., *Enhanced Nutrient Release and Microbial Activity: Assessment of Ca-P mineral enriched biochar loaded with Paenibacillus mucilaginosus.* Water, Air, & Soil Pollution, 2025. **236**(8): p. 511.
52. Marvasi, M., et al., *Bacterial community analysis on the Mediaeval stained glass window "Natività" in the Florence Cathedral.* Journal of Cultural Heritage, 2009. **10**(1): p. 124–133.
53. Schilling, C., et al., *Engineering of the 2,3-butanediol pathway of Paenibacillus polymyxa DSM 365.* Metabolic Engineering, 2020. **61**: p. 381–388.
54. Didak Ljubas, B., et al., *Production of Different Biochemicals by Paenibacillus polymyxa DSM 742 From Pretreated Brewers' Spent Grains.* Frontiers in Microbiology, 2022. **Volume 13 - 2022**.
55. Dias, B.d.C., et al., *2,3-Butanediol production by the non-pathogenic bacterium Paenibacillus brasilensis.* Applied Microbiology and Biotechnology, 2018. **102**(20): p. 8773–8782.
56. Wang, Y., et al., *Metabolism Characteristics of Lactic Acid Bacteria and the Expanding Applications in Food Industry.* Front Bioeng Biotechnol, 2021. **9**: p. 612285.
57. Xiao, Z. and J.R. Lu, *Strategies for enhancing fermentative production of acetoin: A review.* Biotechnology Advances, 2014. **32**(2): p. 492–503.
58. Kurniawan, A., et al., *Characterization of the internal ion environment of biofilms based on charge density and shape of ion.* Colloids and Surfaces B: Biointerfaces, 2015. **136**: p. 22–26.
59. Kurganskaya, I. and A. Luttge, *Mineral Dissolution Kinetics: Pathways to Equilibrium.* ACS Earth and Space Chemistry, 2021. **5**(7): p. 1657–1673.

60. Schott, J., O.S. Pokrovsky, and E.H. Oelkers, *The Link Between Mineral Dissolution/Precipitation Kinetics and Solution Chemistry.* Reviews in Mineralogy and Geochemistry, 2009. **70**(1): p. 207–258.
61. Thorpe, C.L., et al., *Forty years of durability assessment of nuclear waste glass by standard methods.* npj Materials Degradation, 2021. **5**(1): p. 61.
62. Neeway, J., et al., *Dissolution mechanism of the SON68 reference nuclear waste glass: New data in dynamic system in silica saturation conditions.* Journal of Nuclear Materials, 2011. **415**(1): p. 31–37.
63. White, A.F. and S.L. Brantley, *The effect of time on the weathering of silicate minerals: why do weathering rates differ in the laboratory and field?* Chemical Geology, 2003. **202**(3): p. 479–506.
64. Yun, Y.H. and P.J. Bray, *Nuclear magnetic resonance studies of the glasses in the system Na2O-B2O3-SiO2.* Journal of Non-Crystalline Solids, 1978. **27**(3): p. 363–380.
65. Yun, Y.H., S.A. Feller, and P.J. Bray, *Correction and addendum to "Nuclear Magnetic Resonance Studies of the Glasses in the System Na2O-B2O3-SiO2".* Journal of Non-Crystalline Solids, 1979. **33**(2): p. 273–277.
66. Marcial, J., et al., *Boron-speciation and aluminosilicate crystallization in alkali boroaluminosilicate glasses along the NaAl1-xBxSiO4 and LiAl1-xBxSiO4 joins.* Journal of Non-Crystalline Solids, 2019. **506**: p. 58–67.
67. Manara, D., A. Grandjean, and D.R. Neuville, *Structure of borosilicate glasses and melts: A revision of the Yun, Bray and Dell model.* Journal of Non-Crystalline Solids, 2009. **355**(50): p. 2528–2531.
68. Geneste, G., F. Bouyer, and S. Gin, *Hydrogen–sodium interdiffusion in borosilicate glasses investigated from first principles.* Journal of Non-Crystalline Solids, 2006. **352**(28): p. 3147–3152.
69. Neeway, J.J., et al., *The dissolution behavior of borosilicate glasses in far-from equilibrium conditions.* Geochimica et Cosmochimica Acta, 2018. **226**: p. 132–148.
70. Perez, A., et al., *Impact of iron chelators on short-term dissolution of basaltic glass.* Geochimica et Cosmochimica Acta, 2015. **162**: p. 83–98.
71. Hu, R., et al., *Weathering of Basalts by Aspergillus sp. FS-4 Strain: Glass Compositions are Prone to Weathering.* Geomicrobiology Journal, 2020. **37**(2): p. 101–109.
72. Xiong, M.Y., E.S. Shelobolina, and E.E. Roden, *Potential for microbial oxidation of ferrous iron in basaltic glass.* Astrobiology, 2015. **15**(5): p. 331–40.
73. Kip, N. and J.A. van Veen, *The dual role of microbes in corrosion.* The ISME Journal, 2015. **9**(3): p. 542–551.
74. Valbi, V., et al., *Impact of a Mn-oxidizing bacterial strain on the dissolution and browning of a Mn-bearing potash-lime silicate glass.* npj Materials Degradation, 2023. **7**(1): p. 20.
75. Wild, B., R. Gerrits, and S. Bonneville, *The contribution of living organisms to rock weathering in the critical zone.* npj Materials Degradation, 2022. **6**(1): p. 98.
76. Dong, H., et al., *A critical review of mineral–microbe interaction and co-evolution: mechanisms and applications.* National Science Review, 2022. **9**(10): p. nwac128.
77. Samuels, T., et al., *Microbial Weathering of Minerals and Rocks in Natural Environments*, in *Biogeochemical Cycles*. 2020. p. 59–79.
78. Bennett , P.C., et al., *Silicates, Silicate Weathering, and Microbial Ecology.* Geomicrobiology Journal, 2001. **18**(1): p. 3–19.
79. Uroz, S., et al., *Mineral weathering by bacteria: ecology, actors and mechanisms.* Trends in Microbiology, 2009. **17**(8): p. 378–387.
80. Sauer, K., et al., *The biofilm life cycle: expanding the conceptual model of biofilm formation.* Nature Reviews Microbiology, 2022. **20**(10): p. 608–620.
81. Dong, H., et al., *Improvement of phosphate solubilizing bacteria Paenibacillus xylanexedens on the growth of Chlorella pyrenoidosa and wastewater treatment in attached cultivation.* Chemosphere, 2022. **306**: p. 135604.

82. He, X., et al. *Effects of an EPS Biosynthesis Gene Cluster of Paenibacillus polymyxa WLY78 on Biofilm Formation and Nitrogen Fixation under Aerobic Conditions*. Microorganisms, 2021. **9**, DOI: 10.3390/microorganisms9020289.
83. Allocati, N., et al., *Die for the community: an overview of programmed cell death in bacteria.* Cell Death & Disease, 2015. **6**(1): p. e1609–e1609.
84. Mohd Din, A.R.J., et al., *Paenibacillus polymyxa Role Involved in Phosphate Solubilization and Growth Promotion of Zea mays Under Abiotic Stress Condition.* Proceedings of the National Academy of Sciences, India Section B: Biological Sciences, 2020. **90**(1): p. 63–71.
85. Mackenzie, F.T. and R. Gees, *Quartz: synthesis at Earth-surface conditions.* Science, 1971. **173**(3996): p. 533–5.
86. 1. Scholze, H., Nature and Structure of Glass, in Glass: Nature, Structure, and Properties, H. Scholze, Editor. 1991, Springer New York: New York, NY. p. 3–155.
2. Karmakar, B., Fundamentals of Glass and Glass Nanocomposites. 2016. p. 3–53.
3. Chopinet, M.-H., The History of Glass, in Springer Handbook of Glass, J.D. Musgraves, J. Hu, and L. Calvez, Editors. 2019, Springer International Publishing: Cham. p. 1–47.
4. Axinte, E., Glasses as engineering materials: A review. Materials & Design, 2011. 32(4): p. 1717–1732.
5. Marcial, J., et al., Hanford low-activity waste vitrification: A review. Journal of Hazardous Materials, 2024. 461: p. 132437.
6. Peterson, R.A., et al., Review of the Scientific Understanding of Radioactive Waste at the U.S. DOE Hanford Site. Environmental Science & Technology, 2018. 52(2): p. 381–396.
7. Zanini, R., et al., A review of glass corrosion: the unique contribution of studying ancient glass to validate glass alteration models. npj Materials Degradation, 2023. 7(1): p. 38.
8. Frankel, G.S., et al., A comparative review of the aqueous corrosion of glasses, crystalline ceramics, and metals. npj Materials Degradation, 2018. 2(1): p. 15.
9. Hench, L.L., CHARACTERIZATION OF GLASS CORROSION AND DURABILITY, in Glass Surfaces, D.E. Day, Editor. 1975, Elsevier. p. 27–39.
10. Lanford, W.A., et al., Hydration of soda-lime glass. Journal of Non-Crystalline Solids, 1979. 33(2): p. 249–266.
11. Beall, G.H., et al., Ion-Exchange in Glass-Ceramics. Frontiers in Materials, 2016. 3.
12. Gin, S., P. Dillmann, and N. Birbilis, Material degradation foreseen in the very long term: the case of glasses and ferrous metals. npj Materials Degradation, 2017. 1(1): p. 10.
13. Gin, S., et al., Aqueous alteration of silicate glass: state of knowledge and perspectives. npj Materials Degradation, 2021. 5(1): p. 42.
14. Addassi, M., H. Hoteit, and E.H. Oelkers, The impact of secondary silicate mineral precipitation kinetics on CO2 mineral storage. International Journal of Greenhouse Gas Control, 2024. 131: p. 104020.
15. Sorint, S.S. and L.P. Jackson, Evaluation of the toxicity characteristic leaching procedure (TCLP) on utility wastes. Nuclear and Chemical Waste Management, 1988. 8(3): p. 217–223.
16. Weaver, J.L., et al., Microbial interactions with silicate glasses. npj Materials Degradation, 2021. 5(1): p. 11.
17. Barker, W.W., S.A. Welch, and J.F. Banfield, Biogeochemical weathering of silicate minerals. Reviews in Mineralogy and Geochemistry, 1997. 35(1): p. 391–428.
18. Cockell, C.S., et al., Alteration textures in terrestrial volcanic glass and the associated bacterial community. Geobiology, 2009. 7(1): p. 50–65.
19. Sharma, S., et al., Microbial Biofilm: A Review on Formation, Infection, Antibiotic Resistance, Control Measures, and Innovative Treatment. Microorganisms, 2023. 11(6).
20. Flemming, H.-C., et al., Biofilms: an emergent form of bacterial life. Nature Reviews Microbiology, 2016. 14(9): p. 563–575.
21. Konopka, A., et al., Environmental controls on the activity of aquifer microbial communities in the 300 area of the Hanford site. Microb Ecol, 2013. 66(4): p. 889–96.

22. Bagnoud, A., et al., Reconstructing a hydrogen-driven microbial metabolic network in Opalinus Clay rock. Nature Communications, 2016. 7(1): p. 12770.
23. Bell, E., et al., Biogeochemical Cycling by a Low-Diversity Microbial Community in Deep Groundwater. Frontiers in Microbiology, 2018. 9.
24. Weber, K.A., L.A. Achenbach, and J.D. Coates, Microorganisms pumping iron: anaerobic microbial iron oxidation and reduction. Nat Rev Microbiol, 2006. 4(10): p. 752–64.
25. Thorpe, C.L., et al., Microbial interactions with phosphorus containing glasses representative of vitrified radioactive waste. Journal of Hazardous Materials, 2024. 462: p. 132667.
26. André, A.C., L. Debande, and B.S. Marteyn, The selective advantage of facultative anaerobes relies on their unique ability to cope with changing oxygen levels during infection. Cellular Microbiology, 2021. 23(8): p. e13338.
27. Amundson, K.K., M.A. Borton, and M.J. Wilkins, Anthropogenic impacts on the terrestrial subsurface biosphere. Nat Rev Microbiol, 2025. 23(3): p. 147–161.
28. Libourel, G., et al., The use of natural and archeological analogues for understanding the long-term behavior of nuclear glasses. Comptes Rendus Geoscience, 2011. 343(2): p. 237–245.
29. Matthews, B.E., et al., Micro- and Nanoscale Surface Analysis of Late Iron Age Glass from Broborg, a Vitrified Swedish Hillfort. Microscopy and Microanalysis, 2023. 29(1): p. 50–68.
30. Plymale, A.E., et al., Niche Partitioning of Microbial Communities at an Ancient Vitrified Hillfort: Implications for Vitrified Radioactive Waste Disposal. Geomicrobiology Journal, 2021. 38(1): p. 36–56.
31. Parker, G.D., et al., Molecular Imaging of Microbially Induced Corrosion of Synthetic Archeological Glasses by a Rhizosphere Bacterium. Analytical Chemistry, 2025. 97(26): p. 13872–13880.
32. Weaver, J.L., et al., Pre-Viking Swedish hillfort glass: A prospective long-term alteration analogue for vitrified nuclear waste. International Journal of Applied Glass Science, 2018. 9(4): p. 540–554.
33. Choi, S., et al., Application of pH-dependent environmental protection agency test method 1313 to low-activity nuclear waste glass. Journal of Nuclear Materials, 2025. 614: p. 155858.
34. Valbi, V., et al., Bacterial diversity on stained glass windows. International Biodeterioration & Biodegradation, 2023. 177: p. 105529.
35. Verney-Carron, A., et al., Alteration of medieval stained glass windows in atmospheric medium: review and simplified alteration model. npj Materials Degradation, 2023. 7(1).
36. Sterpenich, J. and G. Libourel, Using stained glass windows to understand the durability of toxic waste matrices. Chemical Geology, 2001. 174(1): p. 181–193.
37. Ahmed, B., et al., Fe(III) Reduction and U(VI) Immobilization by Paenibacillus sp. Strain 300A, Isolated from Hanford 300A Subsurface Sediments. Applied and Environmental Microbiology, 2012. 78(22): p. 8001–8009.
38. Marcial, J., et al., Evaluating an EPA leaching test (Method 1313) to relate the long-term performance of nuclear waste glasses and ancient glasses, in Waste Management. 2021: Phoenix, AZ, USA.
39. Marcial, J., et al., Chemical durability assessment of enhanced low-activity waste glasses through EPA method 1313. 2023, Pacific Northwest National Laboratory: Richland, WA, USA. p. 102.
40. McGrail, B.P., et al., Measurement of kinetic rate law parameters on a Na-Ca-Al borosilicate glass for low-activity waste. Journal of Nuclear Materials, 1997. 249(2): p. 175–189.
41. Lee, J.-H., et al., An autotrophic H2-oxidizing, nitrate-respiring, Tc(VII)-reducing Acidovorax sp. isolated from a subsurface oxic-anoxic transition zone. Environmental Microbiology Reports, 2015. 7(3): p. 395–403.
42. Bacon, D.H., et al., Field-Scale Lysimeter Studies of Low-Activity Waste Form Degradation. 2018: United States.
43. Berghouse, M., et al., Advection-dominated transport dynamics of pili and flagella-mediated motile bacteria in porous media. Soft Matter, 2025. 21(18): p. 3622–3637.

44. Ingham, C.J., et al., Mutually facilitated dispersal between the nonmotile fungus Aspergillus fumigatus and the swarming bacterium Paenibacillus vortex. Proc Natl Acad Sci U S A, 2011. 108(49): p. 19731–6.
45. Lee, J.-H., et al., Microbial Reductive Transformation of Phyllosilicate Fe(III) and U(VI) in Fluvial Subsurface Sediments. Environmental Science & Technology, 2012. 46(7): p. 3721–3730.
46. Grady, E.N., et al., Current knowledge and perspectives of Paenibacillus: a review. Microbial Cell Factories, 2016. 15(1): p. 203.
47. Wang, Y.L., et al., Isolation and characterization of mineral-dissolving bacteria from different levels of altered mica schist surfaces and the adjacent soil. World Journal of Microbiology and Biotechnology, 2018. 35(1): p. 2.
48. Deo, N. and K.A. Natarajan, Studies on interaction of Paenibacillus polymyxa with iron ore minerals in relation to beneficiation. International Journal of Mineral Processing, 1998. 55(1): p. 41–60.
49. Parker, G.D., et al., Studying microbially induced corrosion on glass using ToF-SIMS. Biointerphases, 2024. 19(5): p. 051004.
50. Liu, D., B. Lian, and H. Dong, Isolation of Paenibacillus sp. and Assessment of its Potential for Enhancing Mineral Weathering. Geomicrobiology Journal, 2012. 29(5): p. 413–421.
51. Qi, Y., et al., Enhanced Nutrient Release and Microbial Activity: Assessment of Ca-P mineral enriched biochar loaded with Paenibacillus mucilaginosus. Water, Air, & Soil Pollution, 2025. 236(8): p. 511.
52. Marvasi, M., et al., Bacterial community analysis on the Mediaeval stained glass window "Natività" in the Florence Cathedral. Journal of Cultural Heritage, 2009. 10(1): p. 124–133.
53. Schilling, C., et al., Engineering of the 2,3-butanediol pathway of Paenibacillus polymyxa DSM 365. Metabolic Engineering, 2020. 61: p. 381–388.
54. Didak Ljubas, B., et al., Production of Different Biochemicals by Paenibacillus polymyxa DSM 742 From Pretreated Brewers' Spent Grains. Frontiers in Microbiology, 2022. Volume 13 - 2022.
55. Dias, B.d.C., et al., 2,3-Butanediol production by the non-pathogenic bacterium Paenibacillus brasilensis. Applied Microbiology and Biotechnology, 2018. 102(20): p. 8773–8782.
56. Wang, Y., et al., Metabolism Characteristics of Lactic Acid Bacteria and the Expanding Applications in Food Industry. Front Bioeng Biotechnol, 2021. 9: p. 612285.
57. Xiao, Z. and J.R. Lu, Strategies for enhancing fermentative production of acetoin: A review. Biotechnology Advances, 2014. 32(2): p. 492–503.
58. Kurniawan, A., et al., Characterization of the internal ion environment of biofilms based on charge density and shape of ion. Colloids and Surfaces B: Biointerfaces, 2015. 136: p. 22–26.
59. Kurganskaya, I. and A. Luttge, Mineral Dissolution Kinetics: Pathways to Equilibrium. ACS Earth and Space Chemistry, 2021. 5(7): p. 1657–1673.
60. Schott, J., O.S. Pokrovsky, and E.H. Oelkers, The Link Between Mineral Dissolution/Precipitation Kinetics and Solution Chemistry. Reviews in Mineralogy and Geochemistry, 2009. 70(1): p. 207–258.
61. Thorpe, C.L., et al., Forty years of durability assessment of nuclear waste glass by standard methods. npj Materials Degradation, 2021. 5(1): p. 61.
62. Neeway, J., et al., Dissolution mechanism of the SON68 reference nuclear waste glass: New data in dynamic system in silica saturation conditions. Journal of Nuclear Materials, 2011. 415(1): p. 31–37.
63. White, A.F. and S.L. Brantley, The effect of time on the weathering of silicate minerals: why do weathering rates differ in the laboratory and field? Chemical Geology, 2003. 202(3): p. 479–506.
64. Yun, Y.H. and P.J. Bray, Nuclear magnetic resonance studies of the glasses in the system Na2O-B2O3-SiO2. Journal of Non-Crystalline Solids, 1978. 27(3): p. 363–380.
65. Yun, Y.H., S.A. Feller, and P.J. Bray, Correction and addendum to "Nuclear Magnetic Resonance Studies of the Glasses in the System Na2O-B2O3-SiO2". Journal of Non-Crystalline Solids, 1979. 33(2): p. 273–277.

66. Marcial, J., et al., Boron-speciation and aluminosilicate crystallization in alkali boroaluminosilicate glasses along the NaAl1-xBxSiO4 and LiAl1-xBxSiO4 joins. Journal of Non-Crystalline Solids, 2019. 506: p. 58–67.
67. Manara, D., A. Grandjean, and D.R. Neuville, Structure of borosilicate glasses and melts: A revision of the Yun, Bray and Dell model. Journal of Non-Crystalline Solids, 2009. 355(50): p. 2528–2531.
68. Geneste, G., F. Bouyer, and S. Gin, Hydrogen–sodium interdiffusion in borosilicate glasses investigated from first principles. Journal of Non-Crystalline Solids, 2006. 352(28): p. 3147–3152.
69. Neeway, J.J., et al., The dissolution behavior of borosilicate glasses in far-from equilibrium conditions. Geochimica et Cosmochimica Acta, 2018. 226: p. 132–148.
70. Perez, A., et al., Impact of iron chelators on short-term dissolution of basaltic glass. Geochimica et Cosmochimica Acta, 2015. 162: p. 83–98.
71. Hu, R., et al., Weathering of Basalts by Aspergillus sp. FS-4 Strain: Glass Compositions are Prone to Weathering. Geomicrobiology Journal, 2020. 37(2): p. 101–109.
72. Xiong, M.Y., E.S. Shelobolina, and E.E. Roden, Potential for microbial oxidation of ferrous iron in basaltic glass. Astrobiology, 2015. 15(5): p. 331–40.
73. Kip, N. and J.A. van Veen, The dual role of microbes in corrosion. The ISME Journal, 2015. 9(3): p. 542–551.
74. Valbi, V., et al., Impact of a Mn-oxidizing bacterial strain on the dissolution and browning of a Mn-bearing potash-lime silicate glass. npj Materials Degradation, 2023. 7(1): p. 20.
75. Wild, B., R. Gerrits, and S. Bonneville, The contribution of living organisms to rock weathering in the critical zone. npj Materials Degradation, 2022. 6(1): p. 98.
76. Dong, H., et al., A critical review of mineral–microbe interaction and co-evolution: mechanisms and applications. National Science Review, 2022. 9(10): p. nwac128.
77. Samuels, T., et al., Microbial Weathering of Minerals and Rocks in Natural Environments, in Biogeochemical Cycles. 2020. p. 59–79.
78. Bennett , P.C., et al., Silicates, Silicate Weathering, and Microbial Ecology. Geomicrobiology Journal, 2001. 18(1): p. 3–19.
79. Uroz, S., et al., Mineral weathering by bacteria: ecology, actors and mechanisms. Trends in Microbiology, 2009. 17(8): p. 378–387.
80. Sauer, K., et al., The biofilm life cycle: expanding the conceptual model of biofilm formation. Nature Reviews Microbiology, 2022. 20(10): p. 608–620.
81. Dong, H., et al., Improvement of phosphate solubilizing bacteria Paenibacillus xylanexedens on the growth of Chlorella pyrenoidosa and wastewater treatment in attached cultivation. Chemosphere, 2022. 306: p. 135604.
82. He, X., et al. Effects of an EPS Biosynthesis Gene Cluster of Paenibacillus polymyxa WLY78 on Biofilm Formation and Nitrogen Fixation under Aerobic Conditions. Microorganisms, 2021. 9, DOI: 10.3390/microorganisms9020289.
83. Allocati, N., et al., Die for the community: an overview of programmed cell death in bacteria. Cell Death & Disease, 2015. 6(1): p. e1609–e1609.
84. Mohd Din, A.R.J., et al., Paenibacillus polymyxa Role Involved in Phosphate Solubilization and Growth Promotion of Zea mays Under Abiotic Stress Condition. Proceedings of the National Academy of Sciences, India Section B: Biological Sciences, 2020. 90(1): p. 63–71.
85. Mackenzie, F.T. and R. Gees, Quartz: synthesis at Earth-surface conditions. Science, 1971. 173(3996): p. 533–5.
86. Napieralski, S.A., et al., Microbial chemolithotrophy mediates oxidative weathering of granitic bedrock. Proceedings of the National Academy of Sciences, 2019. 116(52): p. 26394–26401.
87. Ahmed, E. and S.J.M. Holmström, Microbe–mineral interactions: The impact of surface attachment on mineral weathering and element selectivity by microorganisms. Chemical Geology, 2015. 403: p. 13–23.

88. Guan, N. and L. Liu, Microbial response to acid stress: mechanisms and applications. Applied Microbiology and Biotechnology, 2020. 104(1): p. 51–65.
89. Luo, Q., et al. Metabolic Engineering of Microorganisms to Produce Pyruvate and Derived Compounds. Molecules, 2023. 28, DOI: 10.3390/molecules28031418.
90. Mayer, R.J., et al., Mechanistic Insight into Metal Ion-Catalyzed Transamination. Journal of the American Chemical Society, 2021. 143(45): p. 19099–19111.
91. Cho, M.-J., S.-Y. Park, and C.-G. Kim Acidic Neutralization by Indigenous Bacteria Isolated from Abandoned Mine Areas. Applied Sciences, 2022. 12, DOI: 10.3390/app12073324.
92. Gauvry, E., et al., Knowledge of the physiology of spore-forming bacteria can explain the origin of spores in the food environment. Research in Microbiology, 2017. 168(4): p. 369–378.
93. Kaziūnienė, J., et al. Optimizing the Growth Conditions of the Selected Plant-Growth-Promoting Rhizobacteria Paenibacillus sp. MVY-024 for Industrial Scale Production. Biology, 2022. 11, DOI: 10.3390/biology11050745.
94. Ojovan, M.I. and W.E. Lee, Glassy Wasteforms for Nuclear Waste Immobilization. Metallurgical and Materials Transactions A, 2011. 42(4): p. 837–851.
95. Berezicka, A., et al. Alteration of Sulfur-Bearing Silicate–Phosphate (Agri)Glasses in Soil Environment: Chemical Interactions and Biological Response. Molecules, 2025. 30, DOI: 10.3390/molecules30081790.
96. Nev, O.A., et al., Predicting microbial growth dynamics in response to nutrient availability. PLOS Computational Biology, 2021. 17(3): p. e1008817.
97. Bunker, B.C., Molecular mechanisms for corrosion of silica and silicate glasses. Journal of Non-Crystalline Solids, 1994. 179: p. 300–308.
98. Ehrlich, H.L., How microbes influence mineral growth and dissolution. Chemical Geology, 1996. 132(1): p. 5–9.

Figure Captions

Figure 1. CLSM images with SYBR gold staining (green) of the original biotic and abiotic samples (prior to washing) from the final time point sampling in depleted HOD for A, B) Dark glass; C, D) Join(mid) glass; E, F) Join glass; and G, H) LAWA44 glass. Panels A, C, E, G are the biotic samples, while panels B, D, F, and H are the corresponding abiotic samples. Fluorescence intensity for each biotic/abiotic pair of panels (e.g. A and B) is the same, but it will differ by each glass type (e.g. A, C, E, G). Panels D and H contain precipitated SYBR gold stain (non-biological precipitates that are morphologically different from the octahedral particles in the biotic Join glass sample).

Figure 2. CLSM images with SYBR gold staining (green) of the original samples (prior to washing) from the final time point sampling in VZPW-amended for A, B) Join glass; C, D) Join(mid) glass; E, F) tumbled LAWA44 glass; and G, F) static LAWA44 glass. Panels A, C, E, G are the biotic samples, while panels B, D, F, and H are the corresponding abiotic samples. Fluorescence intensity for each image is the same.

Figure 3. Concentrations of seven metabolically relevant compounds in depleted HOD solutions, including (A) acetate, (B) acetoin, (C) butyrate, (D) ethanol, (E) formate, (F) lactate (left axis), and glucose (right axis). Plots show the tumbled solutions collected from 2, 49, and 200-day sampling points in the first three sets (Day 2, 49, 200), the Join(mid) glass at 100-day sampling in the fourth set, and the LAWA44 glass at 100-day sampling in the last set, listed from left to right on the X-axis.

Figure 4. NMR analysis of bacteria plus VZPW-amended based glass sample supernatants revealed evidence of seven metabolically relevant compounds, including (A) acetate, (B) acetoin, (C) butyrate, (D) ethanol, (E) formate, (F) lactate (left axis), and glucose (right axis). All graphs

depict the tumbled testing data from glasses in VZPW-amended media collected from 2, 49, and 200-day sampling points in the first three sets (Day 2, 49, 200) and the Join(mid) glass at 100-day sampling in the fourth set, listed from left to right on the X-axis.

Figure 5. Normalized release of boron vs time in each solution for A) Join(mid) glass, B) Join glass, and C) LAWA44 glass. The Dark glass did not contain boron. Inserts provide the same data on a smaller scaled y-axis so that individual trends can be viewed alongside the overall trends in panels A-C. Error bars represent the standard deviation of averaged normalized elemental release of experimental replicates as follows: four replicates at 2 days, three replicates at 4 to 49 days, and two replicates at 100 and 200 days. Some error bars are smaller than the symbol shown.

Figure 6. Normalized release for iron vs time in each solution for A) Dark glass, B) Join(mid) glass, C) Join glass, and D) LAWA44 glass. Inserts provide the same data on a smaller scaled y-axis so that individual trends can be viewed alongside the overall trends in panels A-D. Error bars represent the standard deviation of averaged normalized elemental release of experimental replicates as follows: four replicates at 2 days, three replicates at 4 to 49 days, and two replicates at 100 and 200 days. Some error bars are smaller than the symbol shown.

Figure 7. Normalized release for sodium vs time in each solution for A) Dark glass, B) Join(mid) glass, C) Join glass, and D) LAWA44 glass. Inserts provide the same data on a smaller scaled y-axis so that individual trends can be viewed alongside the overall trends in panels A-D. Error bars represent the standard deviation of averaged normalized elemental release of experimental replicates as follows: four replicates at 2 days, three replicates at 4 to 49 days, and two replicates at 100 and 200 days. Some error bars are smaller than the symbol shown.

Figure 8. Normalized release for silicon vs time in each solution for A) Dark glass, B) Join(mid) glass, C) Join glass, and D) LAWA44 glass. Inserts provide the same data on a smaller scaled y-axis so that individual trends can be viewed alongside the overall trends in panels A-D. Error bars represent the standard deviation of averaged normalized elemental release of experimental replicates as follows: four replicates at 2 days, three replicates at 4 to 49 days, and two replicates at 100 and 200 days. Some error bars are smaller than the symbol shown.

Figure 9. Schematic of experimental setup (not to scale). Glass powders and Paenibacillus were added or excluded, according to the sample matrix, to tubes containing the testing solution (DIW, depleted HOD, or VZPW-amended) and the tubes were tumbled end-over-end at 30 rpm. At pre-determined sampling points, the solutions and solids were separated and sent for liquid (pH, optical density, ICP-OES, NMR) and solids characterization (CLSM).

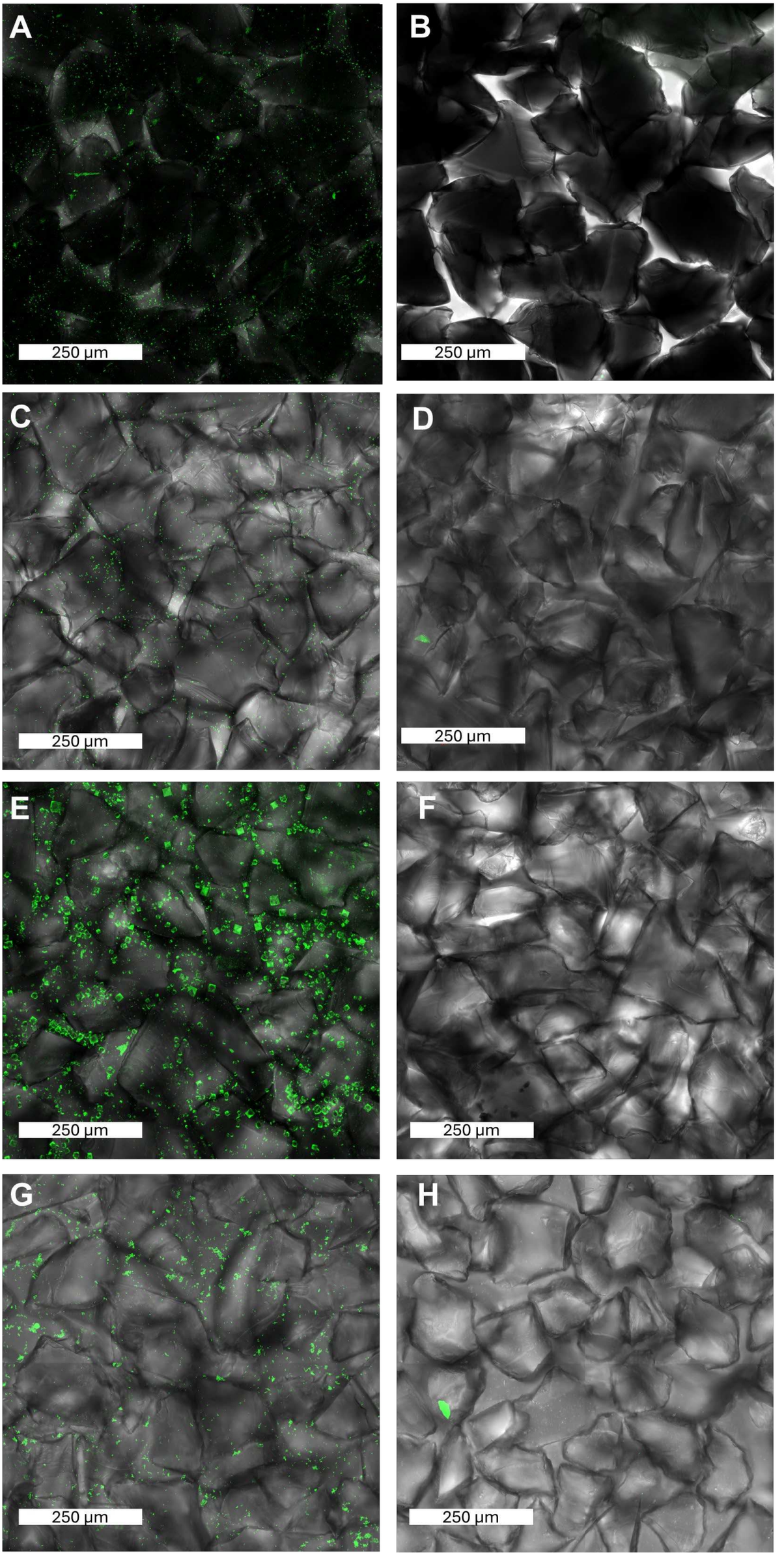
A
250 µm
B
250 µm
C
250 µm
D
250 µm
E
250 µm
F
250 µm
G
250 µm
H
250 µm

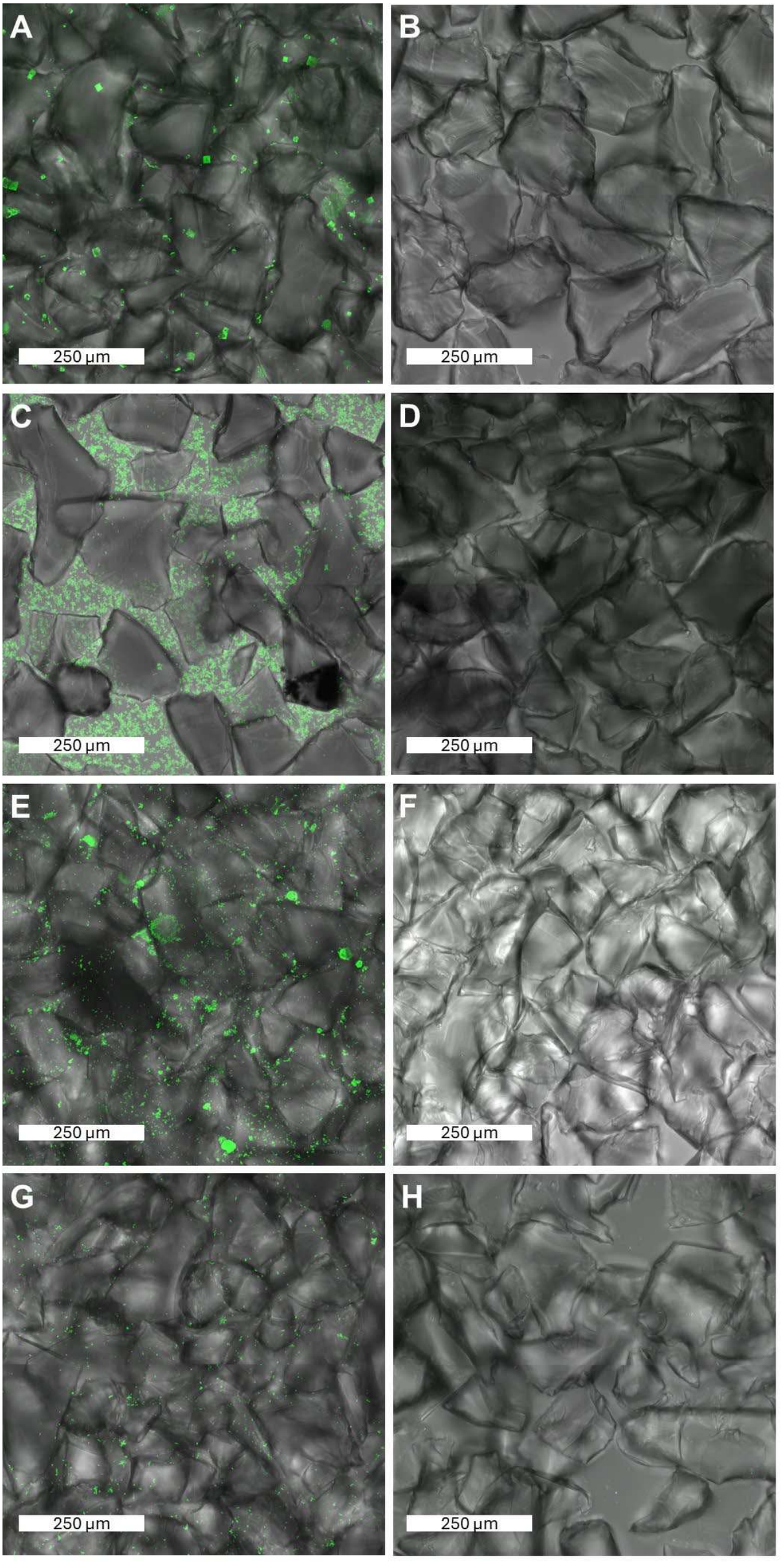
A
250 µm
B
250 µm
C
250 µm
D
250 µm
E
250 µm
F
250 µm
G
250 µm
H
250 µm

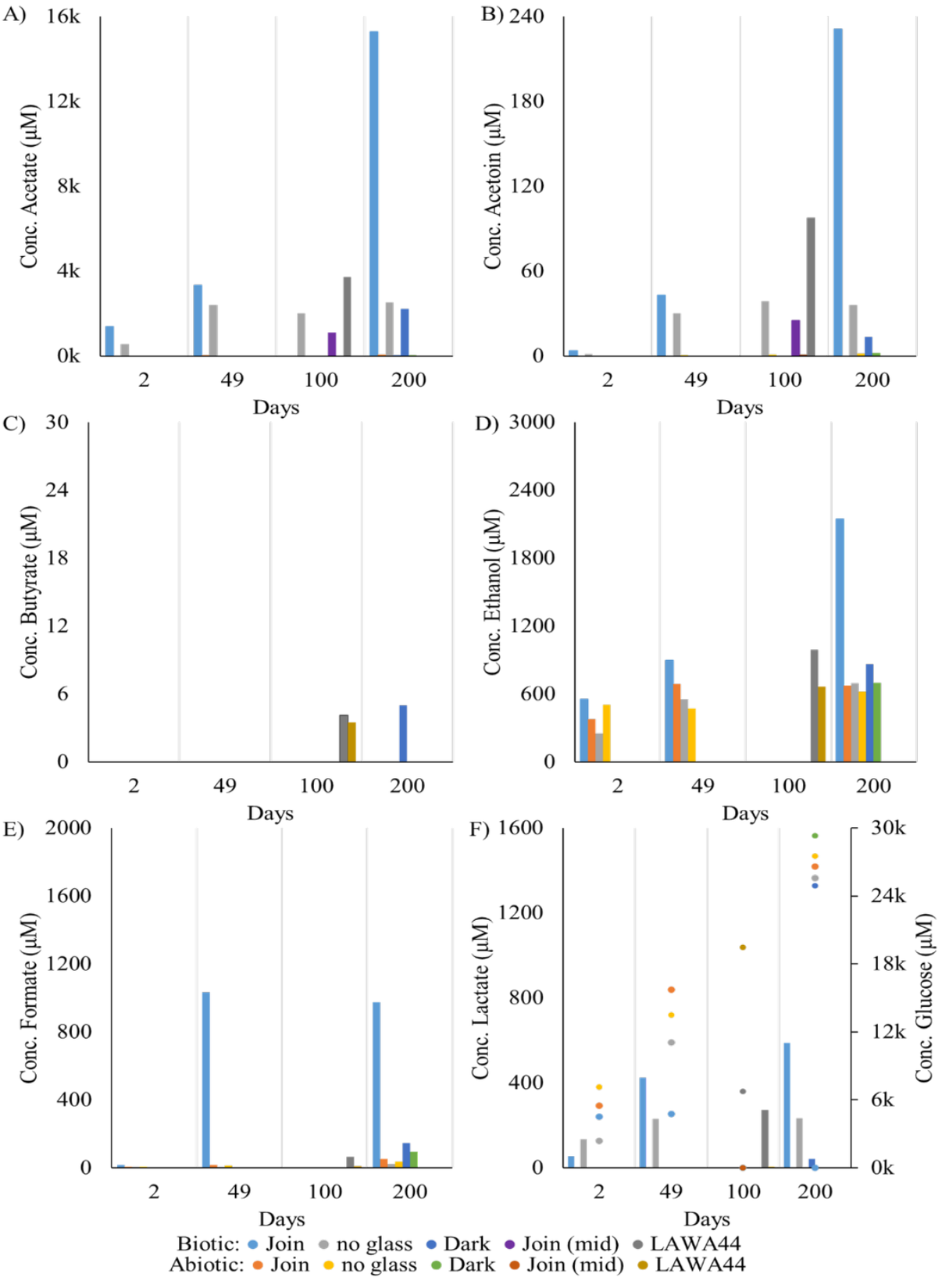
A)
Conc. Acetate (µM)
16k
12k
8k
4k
0k
2
49
100
200
Days
B)
Conc. Acetoin (µM)
240
180
120
60
0
C)
Conc. Butyrate (µM)
30
24
18
12
6
0
D)
Conc. Ethanol (µM)
3000
2400
1800
1200
600
0
E)
Conc. Formate (µM)
2000
1600
1200
800
400
0
F)
Conc. Lactate (µM)
1600
1200
800
400
0
Conc. Glucose (µM)
30k
24k
18k
12k
6k
0k
Biotic: Join no glass Dark Join (mid) LAWA44
Abiotic: Join no glass Dark Join (mid) LAWA44

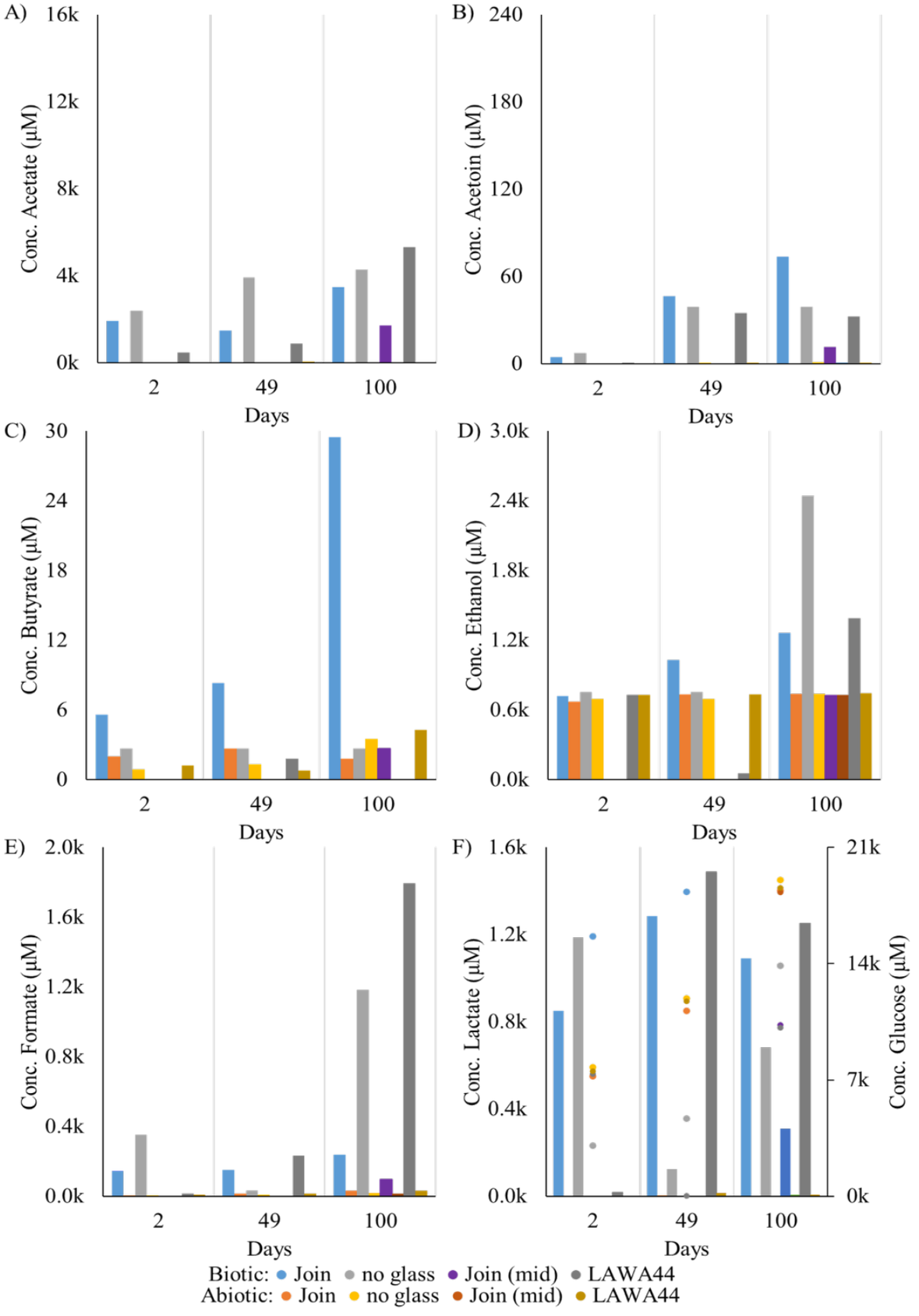
A)
Conc. Acetate (µM)
16k
12k
8k
4k
0k
2
49
100
Days
B)
Conc. Acetoin (µM)
240
180
120
60
0
2
49
100
Days
C)
Conc. Butyrate (µM)
30
24
18
12
6
0
2
49
100
Days
D)
Conc. Ethanol (µM)
3.0k
2.4k
1.8k
1.2k
0.6k
0.0k
2
49
100
Days
E)
Conc. Formate (µM)
2.0k
1.6k
1.2k
0.8k
0.4k
0.0k
2
49
100
Days
F)
Conc. Lactate (µM)
1.6k
1.2k
0.8k
0.4k
0.0k
Conc. Glucose (µM)
21k
14k
7k
0k
2
49
100
Days
Biotic: Join no glass Join (mid) LAWA44
Abiotic: Join no glass Join (mid) LAWA44

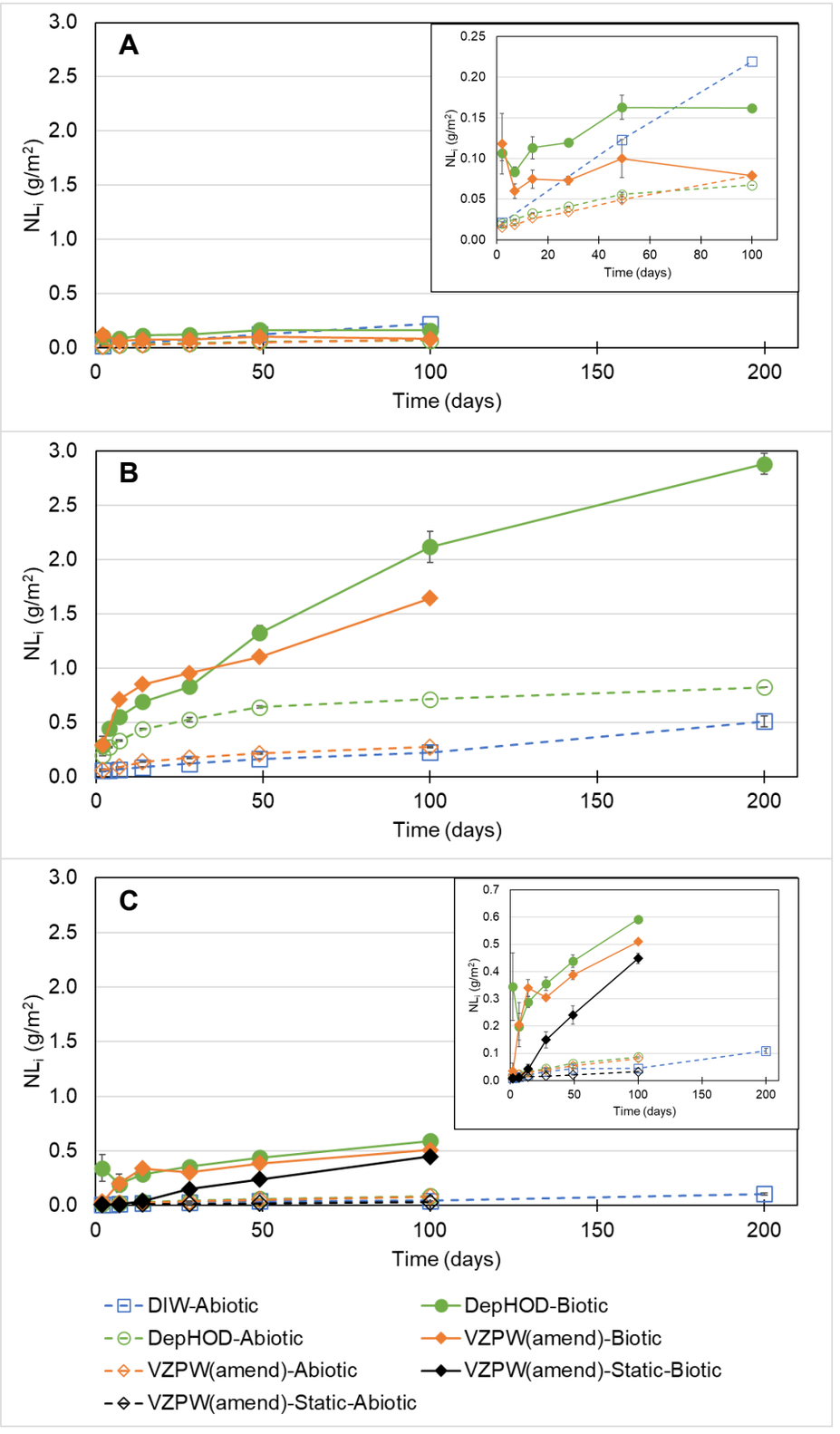
A
B
C
NLi (g/m2)
Time (days)
DIW-Abiotic
DepHOD-Abiotic
VZPW(amend)-Abiotic
VZPW(amend)-Static-Abiotic
DepHOD-Biotic
VZPW(amend)-Biotic
VZPW(amend)-Static-Biotic

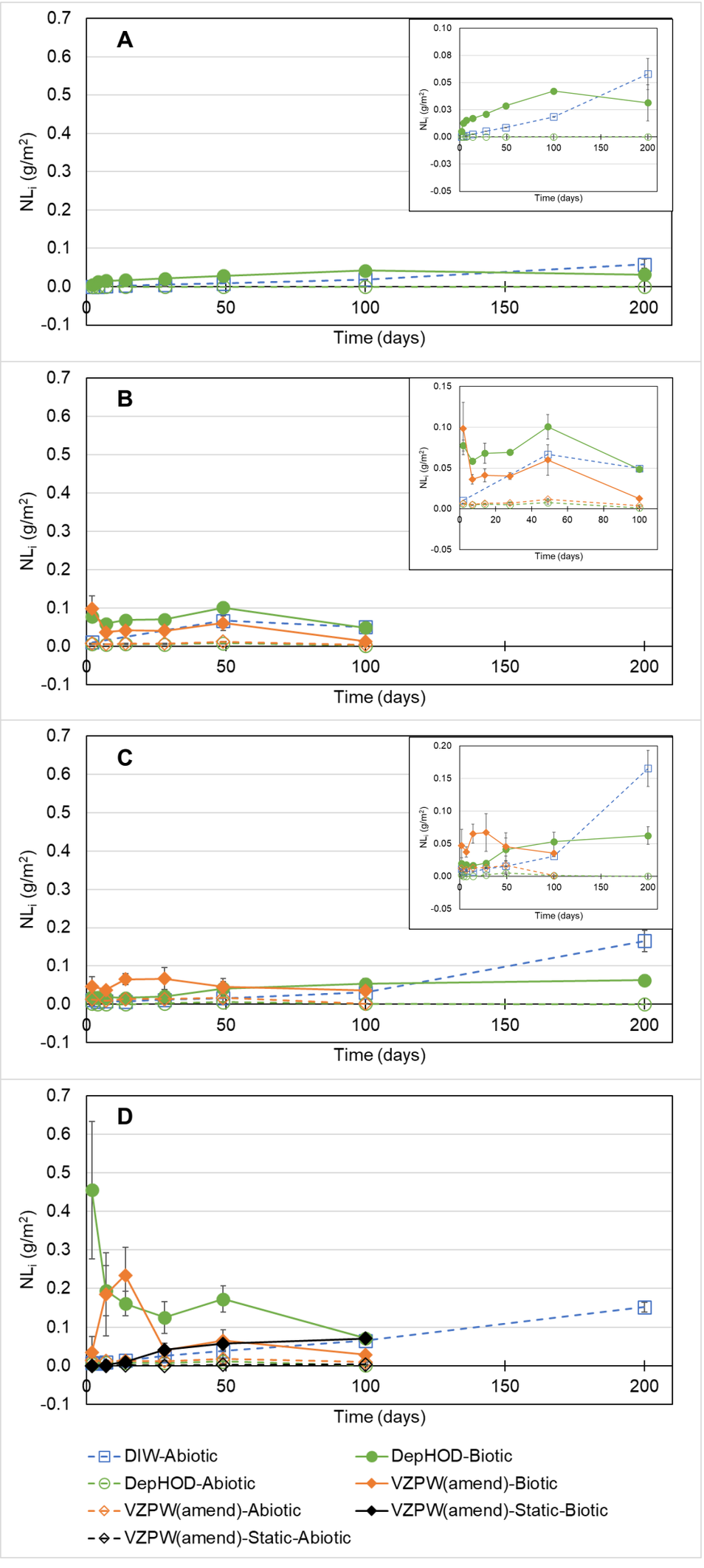
A
B
C
D
NLi (g/m2)
Time (days)
DIW-Abiotic
DepHOD-Abiotic
VZPW(amend)-Abiotic
VZPW(amend)-Static-Abiotic
DepHOD-Biotic
VZPW(amend)-Biotic
VZPW(amend)-Static-Biotic

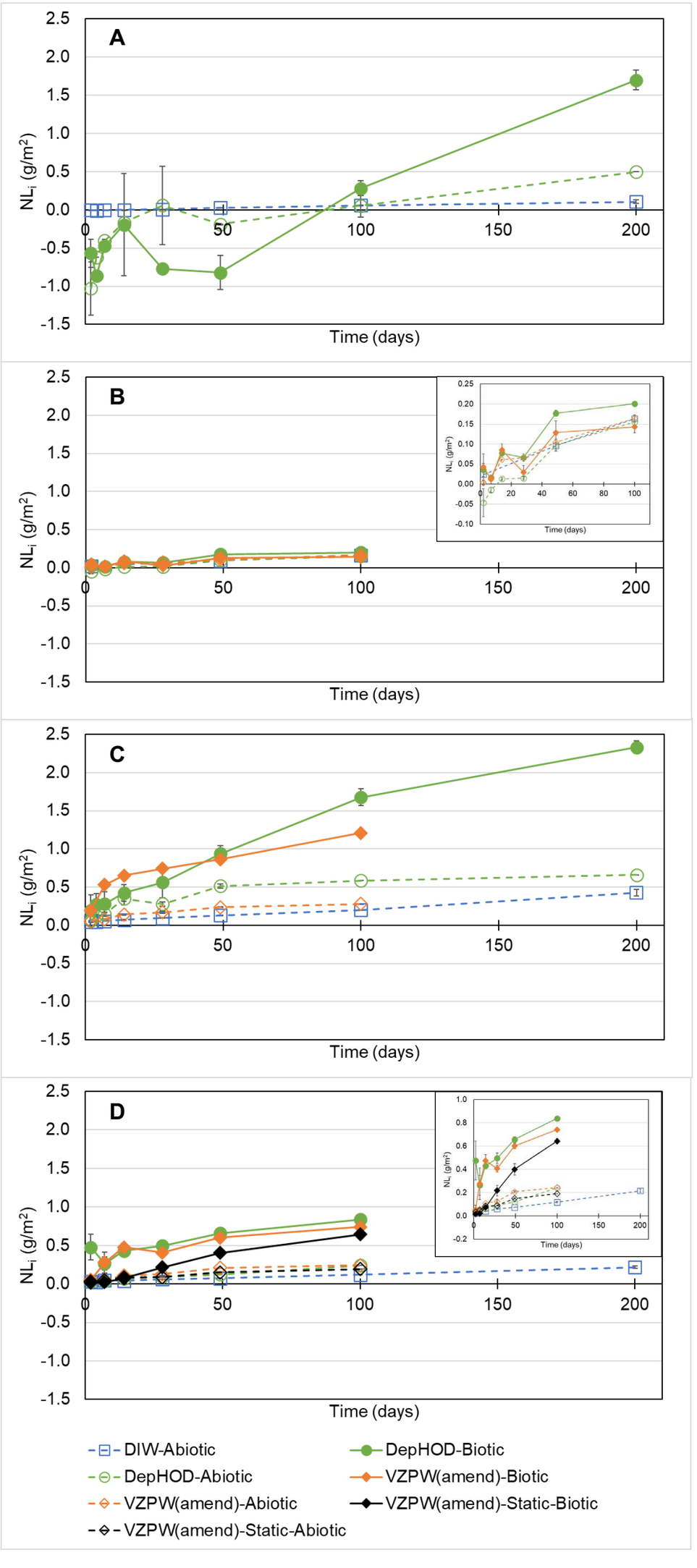
A
B
C
D
NLi (g/m2)
Time (days)
DIW-Abiotic
DepHOD-Abiotic
VZPW(amend)-Abiotic
VZPW(amend)-Static-Abiotic
DepHOD-Biotic
VZPW(amend)-Biotic
VZPW(amend)-Static-Biotic

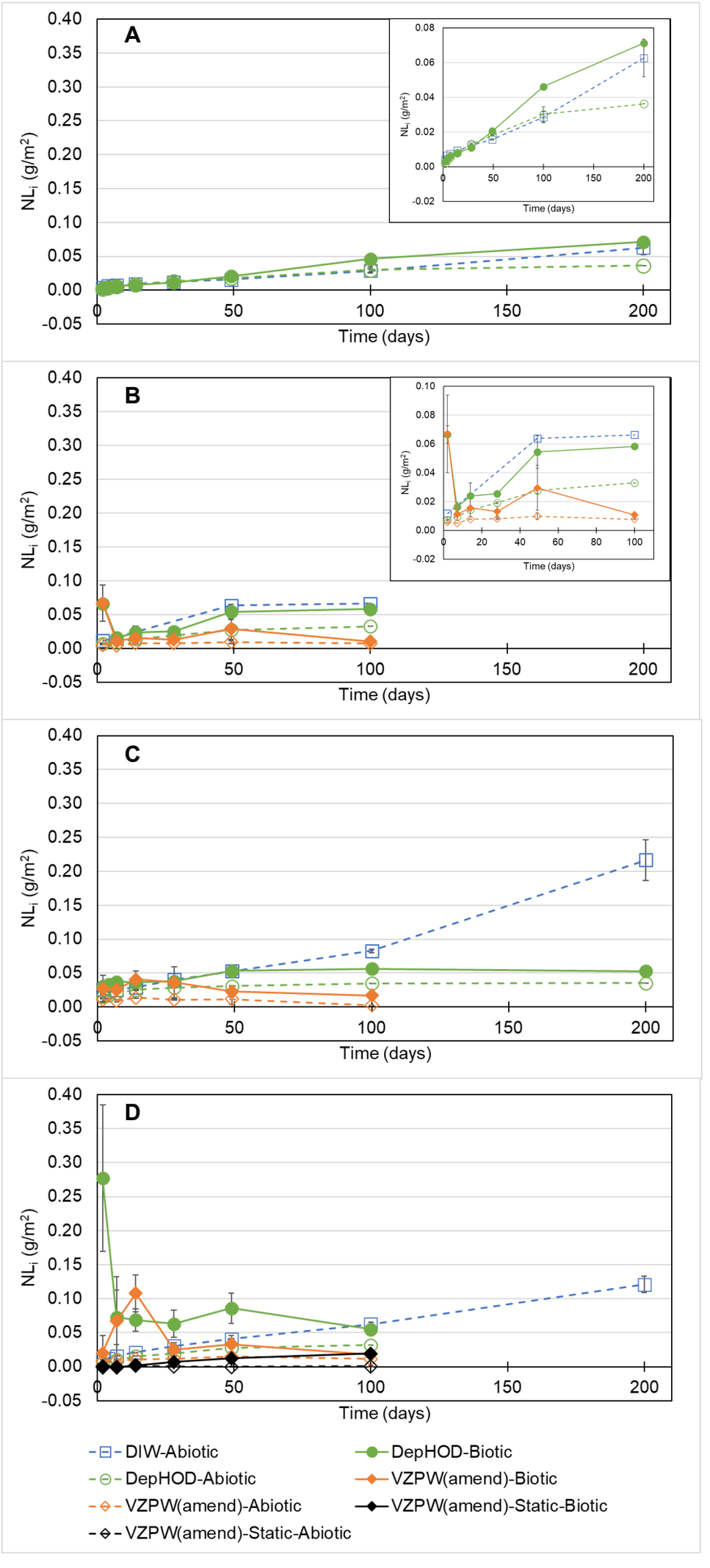
A
B
C
D
NLi (g/m2)
Time (days)
DIW-Abiotic
DepHOD-Abiotic
VZPW(amend)-Abiotic
VZPW(amend)-Static-Abiotic
DepHOD-Biotic
VZPW(amend)-Biotic
VZPW(amend)-Static-Biotic

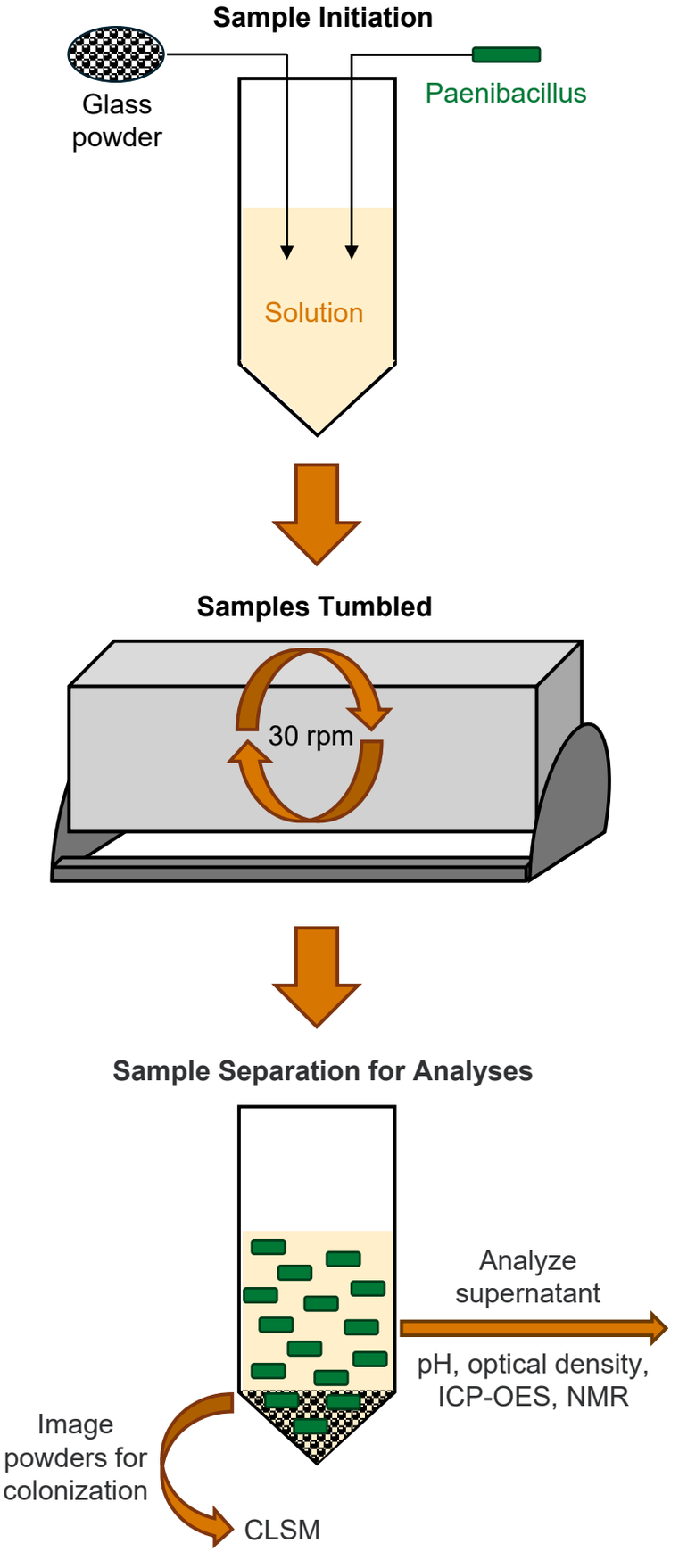
Sample Initiation
Glass powder
Paenibacillus
Solution
Samples Tumbled
30 rpm
Sample Separation for Analyses
Analyze supernatant
pH, optical density, ICP-OES, NMR
Image powders for colonization
CLSM